the effects of moderate hypothermia on the NE efflux evoked by ouabain, tyramine, and cyanide.

MATERIALS AND METHODS

Animal preparation

Animal care proceeded in strict accordance with the guiding principles of the Physiological Society of Japan. Thirty-eight adult cats of either sex (2.1–4.3 kg) were anesthetized with pentobarbital sodium (an initial dose of 30–35 mg/kg intraperitoneally, followed by the maintenance dose of 1–2 mg/kg per h intravenously). The animals were intubated and ventilated with a constant-volume respirator. The heart rate, arterial pressure, electrocardiogram and esophageal temperature were monitored. After left-side thoracotomy, one or two dialysis probes were implanted in the left ventricle free wall using a fine guiding needle. Heparin sodium (100 U/kg) was intravenously administered to prevent blood coagulation.

Dialysis technique and norepinephrine measurement

Using the dialysis technique, the cardiac dialysate NE levels were measured as an index of NE output at the cardiac sympathetic nerve endings. The materials employed and characteristics of the procedure are described elsewhere (8). Briefly, a dialysis fiber (13 mm × 0.2 mm I.D.; PAN-1200, 50000 molecular weight cut-off: Asahi Chemical, Tokyo, Japan) was glued at both ends to a polyethylene tube. The dialysis probes were perfused with Ringer solution (composition: NaCl, 147 m*M*; KCl, 4.0 m*M*; $CaCl_2$, 2.5 m*M*; pH 6.4) at a rate of 10 μl/min. To minimize the influence of tissue injury after the implantation of the dialysis fiber, dialysate sampling was started 120 min after implantation of the dialysis probe (8).

After removing interfering compounds of the dialysate by an alumina procedure, we measured NE concentrations using high-performance liquid chromatography with electrochemical detection (Eicom, Kyoto, Japan) (9).

Experimental protocols

We used several pharmacological agents considered to induce non-exocytotic NE release. Ouabain induces NE release via the NE transporter by the inhibition of the membrane Na^+–K^+ ATPase (10). Tyramine displaces NE toward the axoplasma and the extraneuronal space by an accelerated exchange diffusion mechanism (11). Cyanide intoxication, which has been used as a model of energy depletion, causes non-exocytotic NE release (6). Doses of these pharmacological agents were matched with those used in our previous studies regarding non-exocytotic NE release at cardiac sympathetic nerve endings (12–14).

Protocol 1: effect of desipramine on ouabain-induced, tyramine-induced and cyanide-induced norepinephrine efflux

We used three different types of NE efflux preparations (ouabain, tyramine and cyanide). We collected a baseline dialysate sample using the perfusate of Ringer solution. We then replaced the perfusate with Ringer solution containing ouabain (100 μ*M*), thereby locally administering ouabain through the dialysis probe. The dialysate NE response to ouabain was expressed as the changes in dialysate NE from the basal dialysate NE level. To ensure that the efflux evoked by ouabain is used as a preparation of non-exocytotic NE release, we examined whether the ouabain-induced NE efflux was mainly due to carrier-mediated outward NE transport. The local ouabain administration was performed in vehicle (Ringer solution), and the pre-treatment was performed with local administration of desipramine (membrane NE transport blocking agent, 100 μ*M*). As a similar preparation in separate cats, we measured dialysate NE responses to cyanide (30 m*M*) or tyramine (600 μ*M*) whether desipramine was absent or present.

Protocol 2: effect of ouabain, tyramine and cyanide on the dialysate norepinephrine response during normothermia and hypothermia

We examined the effect of moderate hypothermia on ouabain-induced, tyramine-induced and cyanide-induced NE efflux. The dialysate NE responses to local ouabain, tyramine and cyanide were evoked in normothermia and in moderate hypothermia. After the surgical preparation, surface cooling with an ice pack was performed until the esophageal temperature reached 30°C. When the esophageal temperature did not fall and reached an almost steady-state level, the control dialysate was sampled. Thereafter, Ringer solution containing ouabain (100 μ*M*) was locally administered through the dialysis probe, and we measured the dialysate NE levels during 60 min of administration. In separate cats, the dialysate NE response to cyanide or tyramine was measured under moderate hypothermia.

Statistical analysis

An unpaired *t* test was applied to analyze the differences in the dialysate NE responses with and without the pre-treatment with desipramine in protocol 1. Furthermore, a similar test was applied to analyze the differences in the dialysate NE responses between the normothermia and hypothermia groups in protocol 2. Statistical significance was defined as $p < 0.05$. Values are presented as the mean ± standard error.

RESULTS

Hemodynamic changes and esophageal temperature

Moderate hypothermia induced a decrease in the heart rate but did not alter the mean arterial pressure. Under normothermic or hypothermic conditions, local administration of ouabain, tyramine and cyanide did not alter the heart rate or mean arterial pressure regardless of the presence or absence of desipramine. We measured the esophageal temperature as the core temperature. The core temperature was 37.8 ± 0.4 and 27.4 ± 0.2°C at normothermia and hypothermia, respectively.

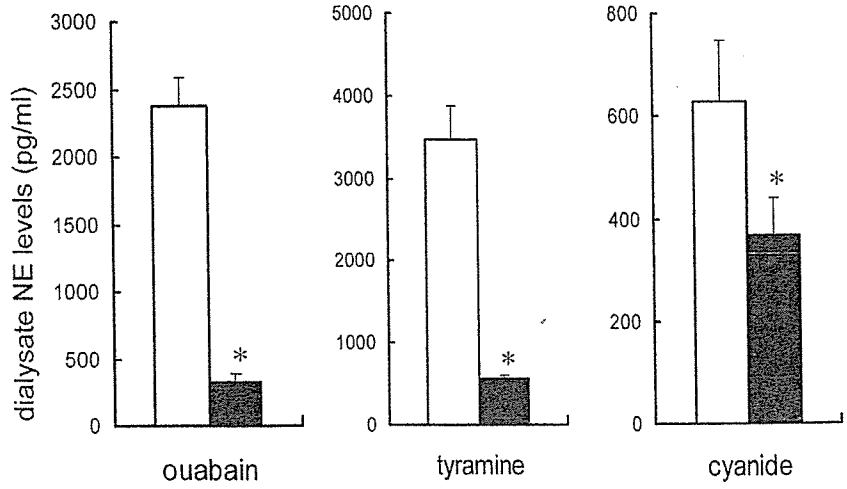

FIG. 1. Effect of desipramine on the efflux evoked by ouabain (100 μ*M*), cyanide (30 m*M*), and tyramine (600 μ*M*). Desipramine suppressed the norepinephrine (NE) efflux evoked by ouabain, cyanide and tyramine. White bar, vehicle; black bar, desipramine pre-treatment. Values presented as mean ± SE (for each group, n = 6). * $p < 0.05$ (versus vehicle).

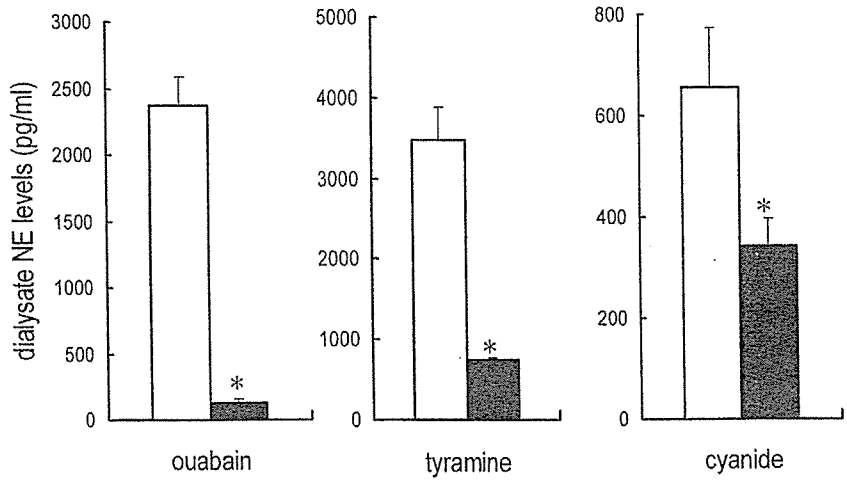

FIG. 2. Effect of moderate hypothermia on the norepinephrine (NE) efflux evoked by ouabain (100 μ*M*), cyanide (30 m*M*) and tyramine (600 μ*M*). Moderate hypothermia suppressed the NE efflux evoked by ouabain, cyanide and tyramine. Coronary occlusion induced the dialysate NE responses. White bar, normothermia; black bar, moderate hypothermia. Values presented as mean ± SE (for each group, n = 6). * $p < 0.05$ (versus normothermia).

Dialysate norepinephrine levels

Protocol 1: effect of ouabain, tyramine and cyanide on the dialysate norepinephrine response with and without desipramine

Basal dialysate NE levels averaged 38 ± 7 pg/ml. Figure 1 shows the ouabain-induced, tyramine-induced and cyanide-induced dialysate NE changes from the basal dialysate NE levels. Local administration of ouabain, tyramine and cyanide caused marked increases in the dialysate NE levels. Desipramine increased the basal dialysate NE levels to 146 ± 12 pg/ml. Desipramine pre-treatment significantly suppressed the NE efflux evoked by ouabain, tyramine, and cyanide.

Protocol 2: effect of ouabain, tyramine and cyanide on the dialysate norepinephrine response during normothermia and hypothermia

Figure 2 shows the ouabain-induced, tyramine-induced and cyanide-induced dialysate NE responses during normothermia and hypothermia. Hypothermia decreased the basal dialysate NE levels to 15 ± 3 pg/ml. Hypothermia significantly suppressed the NE efflux evoked by ouabain, tyramine, and cyanide. With regard to the degree of suppression, the ouabain-induced NE efflux was markedly suppressed while that evoked by cyanide was less suppressed by hypothermia.

DISCUSSION

Local administration of ouabain, tyramine and cyanide caused increases in the dialysate NE levels. Desipramine suppressed the NE efflux evoked by ouabain, tyramine and cyanide. We reconfirmed that the ouabain-induced, tyramine-induced and cyanide-induced NE efflux is dependent on the NE transporter, and is predominantly derived by the carrier-mediated outward NE transporter because desipramine binds to the membrane NE transporter and inhibits bi-directional NE transport (15). If the action of desipramine is exerted on the suppression of NE uptake through inward NE transport, desipramine could augment the NE efflux. According to Schomig et al., non-exocytotic NE release is defined as the NE efflux via the membrane NE transporter through the axoplasma. Thus, the ouabain-induced, tyramine-induced and cyanide-induced NE efflux is used as a model of non-exocytotic NE release. These data are consistent with the findings from earlier studies and our previous data with cardiac dialysis (10–14).

Moderate hypothermia suppressed the NE efflux evoked by ouabain, tyramine and cyanide. The cooling process itself did not exhaust the content of NE at the nerve endings (3). Therefore, our results indicate that moderate hypothermia inhibits the carrier-mediated outward NE transport evoked by ouabain, tyramine and cyanide. From previous studies of ischemia or anoxia, carrier-mediated outward NE transport is required to be two processes in the sympathetic nerve terminal consisting of axoplasmic NE elevation and intraneuronal sodium accumulation (5). Our previous study demonstrated that moderate hypothermia induced increases in dialysate dihydroxyphenylglycol levels, suggesting that moderate hypothermia enhanced NE mobilization from the stored NE vesicle to the axoplasma (3). Moderate hypothermia may therefore suppress the accumulation of intraneuronal sodium via sodium transport failure or increased sodium influx. Similar findings were obtained under low temperature (20 and 12°C) in rat hippocampal slices (16). Low temperatures reduced the intracellular sodium influx evoked by veratridine.

Both moderate hypothermia and desipramine suppressed the NE efflux evoked by ouabain, tyramine and cyanide. Furthermore, with both moderate hypothermia and desipramine, the ouabain-induced NE efflux was markedly suppressed, while that evoked by cyanide was less suppressed. In local administration of ouabain, tyramine and cyanide, the reduction in the NE efflux with hypothermia was similar to that with desipramine. These data suggest that moderate hypothermia suppressed the NE efflux via a mechanism similar to that of desipramine. Further studies concerning the similar action sites and mechanisms of desipramine and hypothermia on the NE efflux are warranted.

In conclusion, we examined the effect of desipramine and moderate hypothermia on the NE efflux evoked by ouabain, tyramine and cyanide. Both moderate hypothermia and desipramine suppressed the NE efflux evoked by ouabain, tyramine and cyanide. Moderate hypothermia suppressed the NE efflux to a similar extent to desipramine regardless of whether ouabain, tyramine, or cyanide was administered.

Acknowledgement: This study was by the program for Promotion of Fundamental Studies in Health Science of the Organization for Pharmaceutical Safety and Research.

REFERENCES

1. Paton DM. *The mechanism of neuronal and extraneuronal transport of catecholamines*. New York: Raven Press, 1975.
2. Bittner MA, Holz RW. A temperature-sensitive step in exocytosis. *J Biol Chem* 1992;267:16226–9.
3. Kitagawa H, Akiyama T, Yamazaki T. Effects of moderate hypothermia on in situ cardiac sympathetic nerve endings. *Neurochem Int* 2002;40:235–42.
4. Vizi ES. Different temperature dependence of carrier-mediated (cytoplasmic) and stimulus-evoked (exocytotic) release of transmitter: a simple method to separate the two types of release. *Neurochem Int* 1998;33:359–66.
5. Schömig A, Dart AM, Dietz R, Mayer E, Kübler W. Release of endogenous catecholamines in the ischemic myocardium of the rat. *Circ Res* 1984;55:689–701.
6. Schömig A, Fischer S, Kurz T, Richardt G, Schömig E. Nonexocytotic release of endogenous noradrenaline in the ischemic and anoxic rate heart: mechanism and metabolic requirements. *Circ Res* 1987;60:194–205.
7. Yamazaki T, Akiyama T, Kitagwa H, Takauchi Y, Kawada T, Sunagawa K. A new, concise dialysis approach to assessment of cardiac sympathetic nerve terminal abnormalities. *Am J Physiol* 1997; 272:H1182–7.
8. Akiyama T, Yamazaki T, Ninomiya I. In vivo monitoring of myocardial interstitial norepinephrine by dialysis technique. *Am J Physiol* 1991;261:H1643–7.
9. Yamazaki T, Akiyama T, Shindo T. Routine high-performance liquid chromatographic determination of myocardial interstitial norepinephine. *J Chromatogr B* 1995;670:328–31.
10. Sweadner KJ. Ouabain-induced norepinephrine release from intact rat sympathetic neurons: evidence for carrier-mediated release. *J Neurosci* 1985;9:2397–406.
11. Bönisch H, Trendelenburg U. Mechanism of action of indirectly acting sympathomimetic amines. In: Trendelenburg U, Weiner N, eds. *Handbook of experimental pharmacology. Catecholamine* 1, Berlin: Springer, 1988;90:246–77.
12. Yamazaki T, Akiyama T, Kawada T. Effect of ouabain on in situ cardiac sympathetic nerve endings. *Neurochem Int* 1999;35:439–45.
13. Takauchi Y, Yamazaki T, Akiyma T. Tyramine-induced endogenous noradrenaline efflux from in situ cardiac sympathetic nerve ending in cats. *Acta Physiol Scand* 2000;168:287–93.
14. Yahagi N, Yamazaki T, Akiyama T. Either desipramine or TMB-8 suppresses cyanide-induced norepinephrine efflux from in vivo cardiac sympathetic nerve of cats. *Brain Res* 2000;864:157–61.
15. Schömig E, Michael-Hepp J, Bönisch H. Inhibition of neuronal noradrenaline uptake ($uptake_1$) and desipramine binding by *N*-ethylmaleimide (NEM). *Naunyn-Schmiedebergs Arch Pharmakol* 1988;337:633–6.
16. Garevich Z, Tretter L, Adam-Vizi V, et al. Analysis of high intracellular [Na^+]-induced release of [^3H] noradrenaline in rat hippocampal slices. *Neuroscience* 2001;104:761–8.

ELSEVIER

Neurochemistry International 42 (2003) 261–267

NEUROCHEMISTRY International

www.elsevier.com/locate/neuint

Effects of ketamine on exocytotic and non-exocytotic noradrenaline release

Hirotoshi Kitagawa [a,*], Toji Yamazaki [b], Tsuyoshi Akiyama [b], Hidezo Mori [b], Kenji Sunagawa [c]

[a] *Department of Anesthesia, Nagahama City Hospital, Nagahama, Japan*
[b] *Department of Cardiac Physiology, National Cardiovascular Center, Research Institute, Suita, Japan*
[c] *Department of Cardiovascular Dynamics, National Cardiovascular Center, Research Institute, Suita, Japan*

Received 29 October 2001; received in revised form 23 April 2002; accepted 2 May 2002

Abstract

To characterise ketamine-induced sympathomimetic action, we examined the effects of ketamine on in vivo cardiac sympathetic nerve endings function. Using adult cats given anaesthesia with pentobarbital, dialysis probes were implanted in the left ventricular myocardium and dialysate noradrenaline (NA) concentrations were measured as an indicator of NA output at the cardiac sympathetic nerve endings. Ketamine was locally administered through the dialysis probe, and dialysate NA responses were obtained in the following conditions. (1) In the resting state, ketamine (10 mM) increased dialysate NA concentration. This increase in dialysate NA was not altered by addition of ω-conotoxin GVIA (N-type Ca^{2+} channel blocker) or desipramine (membrane NA uptake blocker). (2) Sympathetic activation by electrical stimulation of the stellate ganglia (ES-SG; exocytotic NA release): ES-SG caused an increase in dialysate NA, which was further augmented by addition of desipramine. During co-administration of desipramine and ketamine, dialysate NA response to ES-SG was smaller than with desipramine alone. Further, there was no significant difference in the dialysate NA response to ES-SG between ketamine and ketamine + desipramine. These data suggested that both exocytosis and NA uptake function were impaired by ketamine. (3) Non-exocytotic NA release by ouabain: ouabain caused increases in dialysate NA. These increases in dialysate NA were suppressed by ketamine, which impaired the membrane outward NA transport evoked by ouabain. We conclude that ketamine impaired exocytotic and non-exocytotic NA release. However, ketamine spontaneously evoked NA efflux that was independent of exocytosis and insensitive to NA transporter.

Keywords: Cat; Exocytosis; Heart; Membrane noradrenaline transport; Sympathetic nerve

1. Introduction

During ketamine anaesthesia, an increase in plasma noradrenaline (NA) concentration was accompanied with increased arterial pressure (Apple et al., 1979). This finding suggested that ketamine has sympathomimetic action. However, Sasao et al. (1996) demonstrated that ketamine suppressed integrated renal sympathetic nerve activity in rabbits. Furthermore, Kienbaum et al. (2000) reported that ketamine suppressed sympathetic discharge to muscle but augmented plasma NA concentrations in man. Conflicting results of the effect of ketamine on sympathetic nerve activity and neurotransmitter release may be explained by ketamine-induced abnormalities at the sympathetic nerve endings. Recently, several studies have demonstrated that ketamine inhibits neuronal NA uptake in cultured adrenal medullary cells (Hara et al., 1998) and isolated ventricular myocardium (Cook et al., 1992). Alternatively, ketamine was reported to induce non-exocytotic NA release at the sympathetic nerve endings in the isolated perfused heart (Saegusa et al., 1986). Both findings can explain an increase in plasma NA in spite of reduced sympathetic nerve activity. However, it is still uncertain which effect plays a critical role at in vivo sympathetic nerve endings.

We focus here on the effects of ketamine on NA kinetics at sympathetic nerve endings. In the previous study, we reported that dialysis technique makes it possible to assess NA release and NA uptake at in vivo cardiac sympathetic nerve endings (Yamazaki et al., 1997). Furthermore, with pharmacological agents, it is possible to dissociate exocytotic and non-exocytotic NA release at the sympathetic nerve endings (Yahagi et al., 1998; Yamazaki et al., 1997). Therefore, using cardiac dialysis technique in the in vivo heart

* Corresponding author. Present address: Department of Anesthesiology, Shiga University of Medical Science, Otsu, Shiga 520-2192, Japan. Tel.: +81-77-548-2281; fax: +81-77-548-2781.
E-mail address: hirotosi@belle.shiga-med.ac.jp (H. Kitagawa).

0197-0186/03/$ – see front matter © 2003 Elsevier Science Ltd. All rights reserved.
PII: S0197-0186(02)00090-6

(Akiyama et al., 1991), the present study was undertaken to examine to what extent local administration of ketamine modulates the neuronal NA release and uptake at the cardiac sympathetic nerve endings. Further, we examined whether ketamine evokes non-exocytotic NA release and how ketamine modulates the non-exocytotic NA release induced by ouabain (Vizi, 1978).

2. Methods

2.1. Animal preparation

Animal care and all procedures were conducted in strict accordance with the guiding principles of the Physiological Society of Japan. Thirty-five adult cats of either sex (2.1–4.1 kg) were used in this study.

Anaesthesia was induced with pentobarbital (30–35 mg/kg i.p.). After tracheal intubation, anaesthesia was maintained with an intravenous infusion of pentobarbital (1–2 mg/kg/h). The animals were immobilised with pancuronium (0.5 mg/h i.v.) and ventilated with room air mixed with oxygen. The tidal volume and respiratory rate were adjusted to maintain arterial carbon dioxide tension. Oesophageal temperature was monitored and kept at 37 °C by means of a heating pad and lamp. The electrocardiogram was recorded with surface electrodes, and arterial pressure and heart rate were simultaneously monitored.

The fifth or sixth rib on the left side was partially removed to expose the heart. One or two dialysis probes were implanted in the left ventricle free wall of the beating heart using a fine guiding needle. Heparin sodium (100 U/kg) was intravenously administered to prevent blood coagulation, and a maintenance dose was given every 2 h. In the case of nerve stimulation, the second rib on both sides was removed, and the regions of the stellate ganglia were exposed through the intercostal space. Cardiac sympathetic nerves were bilaterally transected at the stellate ganglia, and distal ends were stimulated using a nerve stimulator in protocol 2.

2.2. In vivo dialysis technique

We measured dialysate NA concentrations as indices of myocardial interstitial NA concentrations. The material and properties are described elsewhere (Akiyama et al., 1991; Yamazaki et al., 1995). In brief, a dialysis fibre (13 mm length, 0.31 mm o.d., and 0.2 mm i.d.; PAN-1200, 50 000 molecular weight cut-off, Asahi Chemical, Tokyo, Japan) was glued at both ends to a polyethylene tube (20 cm length, 0.5 mm o.d., and 0.2 mm i.d.). The dialysis probes were perfused with Ringer solution at a rate of 10 μl/min using a microinjection pump. To allow the NA concentrations to reach a steady state, the dialysate sampling was started at 120 min after implantation of the dialysis probe. Taking into account the dead space volume between the dialysis membrane and sample tube, we started dialysate sampling. Sampling periods were 4 min in duration (one sampling volume = 40 μl). Each sample was collected in a microtube containing 4 μl of 0.1 N HCl to prevent amine oxidation.

2.3. Experimental protocols

2.3.1. Preliminary studies: dose dependent ketamine-induced dialysate NA responses

We examined the effects of varying doses (100 μM, 1 mM, 10 mM) of ketamine on dialysate NA concentrations in separate cats. The dialysis probe was perfused with Ringer solution containing ketamine and dialysate samples obtained 60 min after starting local administration of ketamine. Ketamine at 10 mM increased dialysate NA concentrations (Fig. 1). This dose was chosen for the following experiments.

2.3.2. Protocol 1: influence of neuronal blocking agents on dialysate NA response evoked by ketamine

The myocardial interstitial NA concentration is mainly determined by NA release and NA uptake at surrounding cardiac sympathetic nerve endings (Eisenhofer et al., 1991; Kitagawa et al., 1998). To test the hypothesis that the ketamine-induced dialysate NA response was mainly

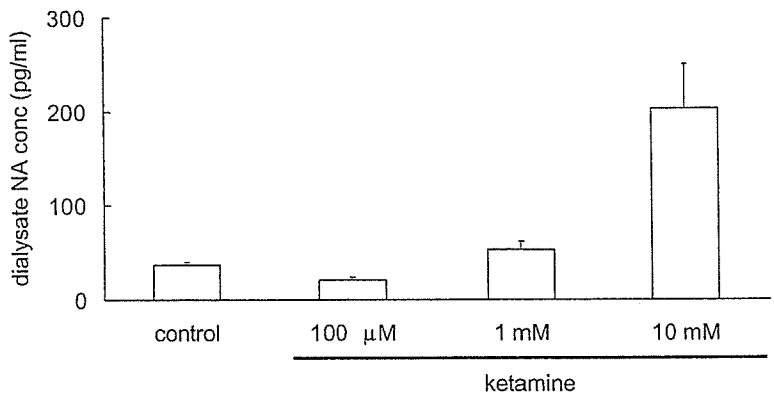

Fig. 1. Effect of varying doses (100 μM, 1 mM, 10 mM) of ketamine on dialysate NA concentrations. Ketamine (10 mM) was locally administered through the dialysis probe and increased dialysate NA concentrations. Values are means ± S.E. ($n = 3$).

involved in exocytotic NA release or impaired NA uptake at the cardiac sympathetic nerve endings, ketamine-induced NA responses were compared with and without either ω-conotoxin GVIA (N-type Ca^{2+} channel blocker: 10 μg/kg i.v.) or desipramine (membrane NA uptake blocker: 100 μM). Furthermore, to test the effect of ketamine on NA release including exocytotis and non-exocytosis (carrier-mediated outward NA transport), the ketamine-induced dialysate NA response was measured with the pretreatment of both ω-conotoxin GVIA and desipramine. Neuropharmacological agents were administered in a separate group of cats. The ketamine-induced dialysate NA response was expressed as the change in dialysate NA from basal concentration.

2.3.3. Protocol 2: influences of ketamine on nerve stimulation-induced dialysate NA responses

To test the modulatory effect of ketamine on exocytotic NA release from in vivo cardiac sympathetic nerve endings, the nerve stimulation-induced dialysate NA responses were measured. Bilateral distal ends of transected stellate ganglia were stimulated consecutively at 5 Hz (10 V, 1 ms in duration) and the dialysate was sampled before and during 4 min nerve stimulation. Dialysate samples were obtained in the presence and absence of ketamine. Furthermore, to test the effect of ketamine on neuronal NA uptake, we compared the nerve stimulation-induced NA responses in the presence and absence of ketamine with desipramine (100 μM) pretreatment. Neuropharmacological agents were administered in a separate group of cats. The ketamine-induced dialysate NA response was expressed as the change in dialysate NA from basal concentration.

2.3.4. Protocol 3: influence of ketamine on ouabain-induced dialysate NA response

To test the modulatory effect of ketamine on non-exocytotic NA release, ouabain-induced NA responses were measured. The previous studies demonstrated that locally applied ouabain caused carrier-mediated outward NA transport (non-exocytotic NA release) from sympathetic nerve endings (Maekawa et al., 2001; Reines et al., 2001; Sumiya et al., 2001; Sweadner, 1985; Vizi, 1978; Yamazaki et al., 1999). Ouabain at 100 μM was locally administered through the dialysis probe, and the dialysate was sampled at 10 min intervals during 60 min administration. Ouabain-induced NA responses were compared with and without pretreatment of ketamine.

The experimental animals were killed at the end of the experiments with an overdose of pentobarbital sodium. We then verified the position of the dialysis probe in the middle layer of the left ventricular myocardium.

2.4. Analytical procedures

Dialysate NA concentrations were measured by high-performance liquid chromatography with electrochemical detection (Eicom, Kyoto, Japan). The chromatographic column consists of a gird column (CA-ODS, 5 mm × 4 mm i.d., Eicom) and analytic reversed-phase column (Eicompack CA-5ODS, 150 mm × 2.1 mm i.d., Eicom). An alumina procedure was performed to remove the interfering compounds from the dialysate (Akiyama et al., 1991). The amperometric detector was operated at 0.40 V versus an Ag/AgCl reference electrode. In the mobile phase, 0.1 M phosphate buffer (pH 6.1) was used with methanol, disodium-EDTA and 1-octanesulfonic acid sodium salt (Yamazaki et al., 1995). The pump flow rate was 0.25 ml/min. The absolute detection limit of NA was 0.1 pg/50 μl injection (signal-to-noise ratio = 3).

2.5. Statistical analysis

One-way analysis variance was applied to analyse differences (Winer, 1971). When statistical significance was detected, the tukey procedure was applied. Unpaired *t*-test was performed to compare the ouabain-induced response of dialysate NA concentrations with and without ketamine. Statistical significance was defined as $P < 0.05$. Values are presented as means ± standard error.

3. Results

3.1. Protocol 1: influence of neuronal blocking agents on dialysate NA response evoked by ketamine

Local administration of ketamine did not affect the changes in systemic hemodynamics or ECG. Ketamine increased dialysate NA concentrations to 137 ± 11 pg/ml at 60 min of ketamine administration. This high concentration was maintained during 120 min administration. The pretreatment with ω-conotoxin GVIA, desipramine and combination of ω-conotoxin GVIA and desipramine altered basal dialysate NA concentrations (Table 1). However, there were no significant differences in ketamine-induced NA responses among these groups (Fig. 2).

Table 1
Basal dialysate NA concentrations

	Dialysate NA concentrations (pg/ml)
Protocol 1	
Vehicle	37 ± 3
ω-Conotoxin GVIA	24 ± 3
Desipramine	91 ± 9
ω-Conotoxin GVIA + desipramine	69 ± 9
Protocol 2 (after transection of stellate ganglia)	
Vehicle	18 ± 5
Desipramine	74 ± 6
Ketamine	135 ± 19
Ketamine + desipramine	183 ± 39

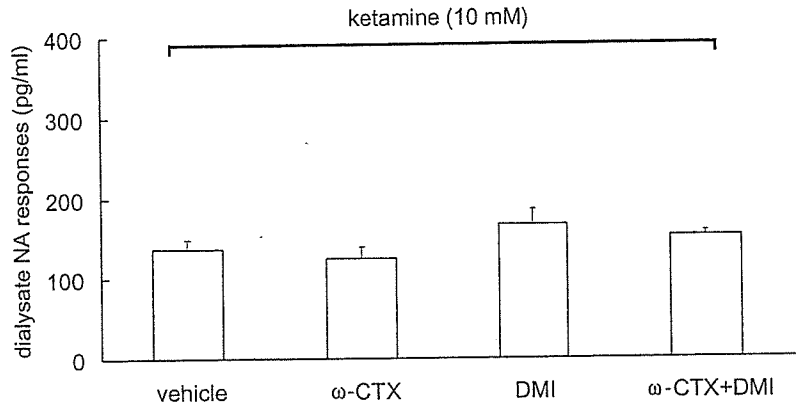

Fig. 2. Ketamine (10 mM)-induced dialysate NA responses in various conditions. Pretreatment with ω-conotoxin GVIA (ω-CTX) and/or desipramine (DMI) did not alter dialysate NA response. Values are means ± S.E. ($n = 5$).

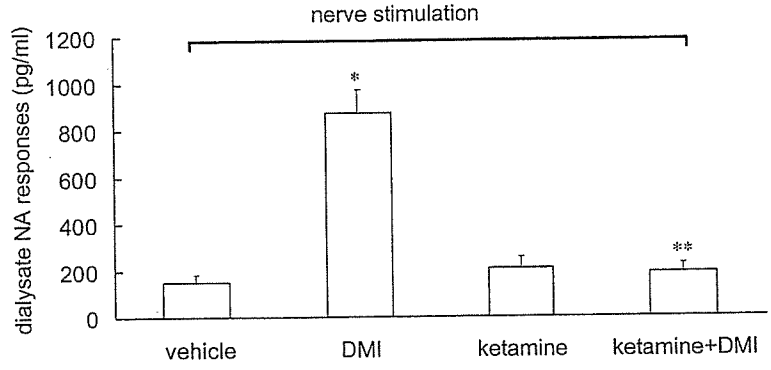

Fig. 3. Effect of ketamine (10 mM) and desipramine (DMI) (100 μM) on dialysate NA responses to electrical stimulation of stellate ganglia (5 Hz, 10 V). Values are means ± S.E. ($n = 6$). *$P < 0.05$ vs. value in vehicle group; **$P < 0.05$ vs. value in desipramine alone group.

3.2. Protocol 2: influences of ketamine on nerve stimulation-induced dialysate NA responses

Electrical stimulation of the stellate ganglia increased dialysate NA concentration to 150 ± 31 pg/ml (Fig. 3). The stimulation-induced NA response was augmented by administration of desipramine. Ketamine pretreatment caused an increase in basal dialysate NA concentrations (Table 1), but the nerve stimulation-induced NA response was not altered in comparison with the vehicle group. Furthermore, with pretreatment of ketamine and desipramine, nerve stimulation-induced NA responses were not altered in comparison with ketamine alone but suppressed in comparison with the desipramine group. These data suggested

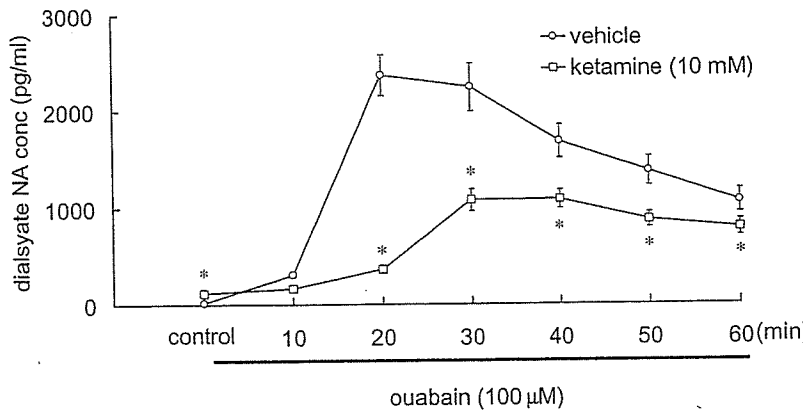

Fig. 4. Time course of dialysate NA concentrations during local administration of ouabain (100 μM) with and without pretreatment of ketamine. Values are means ± S.E. ($n = 6$). *$P < 0.05$ vs. concurrent value in vehicle group.

that ketamine suppressed both exocytotic NA release and NA uptake evoked by the electrical stimulation of cardiac sympathetic nerves.

3.3. Protocol 3: influence of ketamine on ouabain-induced dialysate NA response

Fig. 4 presents the time course of the dialysate NA concentrations during local administration of ouabain (100 μM). In the vehicle group, dialysate NA concentration increased significantly to 2371 ± 215 pg/ml at 20 min during ouabain administration. With the addition of ketamine, ouabain caused increases in dialysate NA. In comparison with the vehicle group, ketamine suppressed the ouabain-induced NA response at 20–60 min during ouabain administration.

4. Discussion

Our result demonstrates that, in an in vivo cat heart, locally applied 10 mM ketamine caused a brisk increase in dialysate NA concentration. This NA increment was not augmented by addition of desipramine. In vitro studies suggested that ketamine inhibited neuronal NA uptake at the sympathetic nerve endings (Cook et al., 1992). If ketamine shares the inhibitory effect of neuronal NA uptake with desipramine via the same binding site (Hara et al., 1998), the absence of any effect of desipramine on ketamine-induced NA efflux may be explained in part by this mechanism. If this is the case, exocytotic NA release was accompanied by subsequent NA uptake inhibition, and ketamine-induced NA efflux could be reduced by addition of ω-conotoxin GVIA. However, ketamine-induced NA efflux was not reduced by pretreatment with ω-conotoxin GVIA. This result indicates that ketamine-induced NA efflux was independent of N-type Ca^{2+} channel opening coupled to exocytosis, and participation of ketamine on the inhibition of neuronal NA uptake may be ruled out. Furthermore, carrier-mediated NA transport was not involved in the change of dialysate NA evoked by ketamine because desipramine blocks carrier-mediated NA transport bi-directionally (Akiyama and Yamazaki, 1999; Yamazaki et al., 1997). Alternatively, ketamine may exert a dual action via exocytosis or neuronal NA transport. Then, the addition of desipramine or ω-conotoxin GVIA only may inhibit each action and residual action may cause a redundant effect on ketamine-induced NA efflux. Pretreatment with ω-conotoxin GVIA and desipramine did not alter ketamine-induced NA efflux. Thus, ketamine-induced NA efflux was independent of N-type Ca^{2+} channel coupled to exocytosis and insensitive to carrier-mediated neuronal NA transport, and might be due to the passive diffusion from the axoplasmic site.

Electrical stimulation of the stellate ganglia caused an increase in dialysate NA concentrations, which was blocked by addition of ω-conotoxin GVIA (Yamazaki et al., 1997). Although ketamine evoked spontaneous NA efflux, nerve-stimulation further facilitated the dialysate NA concentrations by exocytosis. There was no significant difference in the NA response evoked by nerve stimulation between the vehicle and ketamine groups. This result indicates that ketamine did not appear to affect the exocytotic NA release evoked by nerve stimulation. However, with the addition of desipramine and ketamine, the nerve stimulation-induced NA response was suppressed in comparison with the desipramine group. During pretreatment with a neuronal NA uptake blocker such as desipramine, the nerve stimulation-induced dialysate NA response expresses the total amount of exocytotic NA release because subsequent neuronal NA uptake is blocked with desipramine (Eisenhofer et al., 1991; Yamazaki et al., 1997). Therefore, these results indicate that ketamine caused suppression of the exocytotic NA release evoked by electrical stimulation of sympathetic nerves. Furthermore, desipramine did not affect the NA response evoked by nerve stimulation during ketamine administration. This result indicates that ketamine may share the inhibition of neuronal NA uptake with desipramine via the same binding site (Hara et al., 1998). These data suggested that ketamine suppressed exocytotic NA release and NA uptake evoked by the electrical stimulation of the stellate ganglia. The impairment of NA uptake may mask inhibitory action of ketamine on NA release. Only either inhibition of NA release or NA transport did not interpret overall data on the nerve-stimulation.

The suppressive effect of ketamine on exocytotic NA release might be related to its action on the inhibition of Na^+ channel at the surrounding sympathetic axon (Allaoua and Chicheportiche, 1989; Brau et al., 1997). If so, our results (protocol 1 and 2) were consistent with the conflicting results of the effect of ketamine on sympathetic nerve activity and neurotransmitter release in the clinical setting (Apple et al., 1979; Kienbaum et al., 2000). Alternatively, during ketamine administration, the amount of NA efflux from axoplasmic site may be greater that that of membrane NA uptake. Thus, opposing NA efflux may underestimate the amount of neuronal NA uptake. Furthermore, on the result of protocol 1, the lack of effect of ω-conotoxin GVIA and desipramine can be explained in part by this suppression of exocytosis and NA uptake.

Only either inhibition of NA release or NA transport did not interpret overall data on the nerve-stimulation. Ouabain evoked a brisk increase in dialysate NA by inhibition of Na^+-K^+ ATPase. Inhibition of Na^+-K^+ ATPase caused accumulation of intracellular Na^+ which could carry NA out of the axoplasma with NA transporter (Sweadner, 1985; Yamazaki et al., 1999). Ketamine suppressed the increment in dialysate NA response evoked by ouabain. This result indicates that ketamine evoked the inhibition of carrier-mediated NA transport. This action induced by ketamine is similar to that induced by desipramine, with the binding sites possibly the same. Taken together (protocol 2 and 3), our data suggest that ketamine blocks both normal and reverse NA transport.

Although local administration of ketamine acted by releasing NA that was independent of ω-conotoxin GVIA and insensitive to desipramine, ketamine suppressed both the exocytotic NA release evoked by nerve stimulation and non-exocytotic NA release evoked by pharmacological intervention (ouabain). Desipramine insensitive and ω-conotoxin GVIA resistant NA efflux was observed under co-administration of a vesicle NA transport inhibitor (reserpine) and a monoamine oxidase inhibitor (pargyline) (Yamazaki et al., 1997). Co-administration of these agents leads to the mobilization of NA from stored NA vesicle to axoplasma and the accumulation of NA in the axoplasmic site. Ketamine also may displace NA towards the axoplasma and extraneuronal spaces. A similar mechanism was proposed for tyramine-induced NA efflux (Bönisch and Trendelenburg, 1988; Takauchi et al., 2000). However, in the case of tyramine, the neuronal NA transport carrier that transported tyramine into the axoplasma induced the outward transport of NA from axoplasmic site. On the other hand, the neuronal NA transport carrier did not transport ketamine, and NA efflux seems to be derived via passive diffusion, which is an outward chemical gradient for NA. Furthermore, the mobilization of NA from the stored vesicle to the axoplasmic site may lead to exhaustion of NA at the stored NA vesicle. Consequently, exocytotic NA release evoked by nerve stimulation was suppressed. In two different stimulations (perturbation induced exocytotic and non-exocytotic NA release), ketamine seems to inhibit carrier-mediated NA transport bi-directionally. This result may be consistent with the finding that ketamine-induced NA efflux was due to passive diffusion rather than an accelerated exchange diffusion mechanism.

4.1. Methodological considerations

There are several limitations to the present study. First, we investigated myocardial NA concentrations in cats anaesthetised with pentobarbital sodium. Because this barbiturate anaesthesia affects the autonomic nervous system (Hirota et al., 2000), the results might have altered if non-barbiturate anaesthesia or no anaesthesia had been used. Pentobarbital anaesthesia might interact with locally applied ketamine on NA kinetics.

Second, we administered ketamine as a racemate through the dialysate probes. Recently, ketamine has been reported to consist of two isomers, S(+)- and R(−)-ketamine (Hancock and Stamford, 1999; Nishimura and Sato, 1999). Stereospecific effects of ketamine on monoamine kinetic at the nerve ending have been discussed. Complicated results may be dissociated with stereoselectivity. Further studies are clearly required to elucidate the effect of selective isomer on the NA kinetics.

Local administration of ketamine spontaneously evoked NA efflux that was independent of ω-conotoxin GVIA and insensitive to desipramine. Further, ketamine suppressed exocytotic NA release evoked by nerve stimulation and non-exocytotic NA release evoked by pharmacological intervention (ouabain). These results may be explained in part by the suppression by ketamine of sympathetic discharge but augmentation of plasma NA concentrations. Furthermore, these complicated effects of ketamine may gain relevance during ketamine-induced neuroprotection in ischemic brain.

References

Akiyama, T., Yamazaki, T., 1999. Norepinephrine release from cardiac sympathetic nerve endings in the in vivo ischemic region. J. Cardiovasc. Pharmocol. 34 (Suppl. 4), S11–14.

Akiyama, T., Yamazaki, T., Ninomiya, I., 1991. In vivo monitoring of myocardial interstitial norepinephrine by dialysis technique. Am. J. Physiol. 261, H1643–H1647.

Allaoua, H., Chicheportiche, R., 1989. Anaesthetic properties of phencyclidine (PCP) and analogues may be related to their interaction with Na^+ channels. Eur. J. Pharmacol. 25, 327–335.

Apple, E., Dudziak, R., Palm, D., Wnuk, A., 1979. Sympathoneuronal and sympathoadrenal activation during ketamine anesthesia. Eur. J. Clin. Pharmacol. 16, 91–95.

Bönisch, H., Trendelenburg, U., 1988. Mechanism of action of indirectly acting sympathomimetic amines. In: Trendelenburg, U., Weiner, N. (Eds.), Handbook of Experimental Pharmacology, Vol. 90/1. Catecholamine 1, Springer, Berlin, pp. 246–277.

Brau, M.E., Sander, F., Vogel, W., Hempelmann, G., 1997. Blocking mechanisms of ketamine and its enantiomers in enzymatically demyelinated peripheral nerve as revealed by single-channel experiments. Anesthesiology 86, 394–404.

Cook, D.J., Housmans, P.R., Rorie, D.K., 1992. Effect of ketamine HCL on norepinephrine disposition in isolated ferret ventricular myocardium. J. Pharmacol. Exp. Ther. 261, 101–107.

Eisenhofer, G., Smolich, J.J., Cox, H.S., Esler, M.D., 1991. Neuronal reuptake of norepinephrine and production of dihydroxyphenylglycol by cardiac sympathetic nerves in the anesthetized dogs. Circulation 84, 1354–1363.

Hancock, P.J., Stamford, J.A., 1999. Stereospecific effects of ketamine on dopamine efflux and uptake in the rat nucleus accumbens. Br. J. Anaesth. 82, 603–608.

Hara, K., Yanagihara, N., Minami, K., Ueno, S., Toyohira, Y., Sata, T., Kawamura, M., Bruss, M., Bonish, H., Shigematsu, A., Izumi, F., 1998. Ketamine interacts with the noradrenaline transporter at a site partly overlapping the desipramine binding site. Naunyn Schmiedebergs Arch. Pharmacol. 358, 328–333.

Hirota, K., Kudo, M., Kudo, T., Kitayama, M., Kushikata, T., Lambert, D.G., Matsuki, A., 2000. Barbiturates inhibit K(+)-evoked noradrenaline and dopamine release from rat striatal slices—involvement of voltage sensitive Ca(2+) channels. Neurosci. Lett. 291, 175–178.

Kienbaum, P., Heuter, T., Michel, M.C., Peters, J., 2000. Racemic ketamine decreases muscle sympathetic activity but maintains the neuronal response to hypotensive challenges in humans. Anesthesiology 92, 94–101.

Kitagawa, H., Akiyama, T., Yamazaki, T., 1998. Myocardial interstitial noradrenaline monitoring during occlusion of inferior vena cava in cats. Acta Physiol. Scand. 163, 173–179.

Nishimura, M., Sato, K., 1999. Ketamine stereoselectively inhibits rat dopamine transporter. Neurosci. Lett. 272, 131–134.

Maekawa, M., Murayama, T., Nomura, Y., 2001. Involvement of noradrenaline transports in S-nitrosocysteine-stimulated noradrenaline release from rat brain slices: existence of functional Na(+)-independent transport activity. Neurochem. Int. 38, 323–331.

Reines, A., Pena, C., Arnaiz, G., 2001. [^{3}H]Dizocilpine binding to *N*-methyl-D-asparate (NMDA) receptor is modulated by an endogenous Na^+, K^+-ATPase inhibitor. Comparison with ouabain. Neurochem. Int. 39, 301–310.

Saegusa, K., Furukawa, Y., Ogiwara, Y., Chiba, S., 1986. Pharmacologic analysis of ketamine-induced cardiac actions in isolated, blood-perfused canine atria. J. Cardiovasc. Pharmacol. 8, 414–419.

Sasao, J., Taneyama, C., Kohno, N., Goto, H., 1996. The effects of ketamine on renal sympathetic nerve activity and phrenic nerve activity in rabbits (with vagotomy) with and without afferent inputs from peripheral receptors. Anesth. Analg. 82, 362–367.

Sumiya, Y., Torigoe, K., Gerevich, Z., Kofalvi, A., Vizi, E.S., 2001. Excessive release of [^{3}H]noradrenaline by veratridine and ishcmeia in spinal cord. Neurochem. Int. 39, 59–63.

Sweadner, K.J., 1985. Ouabain-evoked norepinephrine release from intact rat sympatheic neurons: evidence for carrier-mediated release. J. Neurosci. 9, 2397–2406.

Takauchi, Y., Yamazaki, T., Akiyama, T., 2000. Tyramine-induced endogenous noradrenaline efflux from in situ cardiac sympathetic nerve ending in cats. Acta Physiol. Scand. 168, 287–293.

Vizi, E.S., 1978. Na^+, K^+ activated adnosinetriphosphate as a trigger in transmitter release. Neuroscience 3, 367–384.

Winer, B.J., 1971. Statistical Principles in Experimental Design, 2nd Edition. McGraw-Hill, New York.

Yahagi, N., Akiyama, T., Yamazaki, T., 1998. Effects of ω-conotoxin GVIA on cardiac sympathetic nerve function. J. Auton. Nerv. Syst. 68, 43–48.

Yamazaki, T., Akiyama, T., Shindo, T., 1995. Routine high-performance liquid chromatographic determination of myocardial interstitial norepinephrine. J. Chromatogr. B Biomed. Appl. 670, 328–331.

Yamazaki, T., Akiyama, T., Kitagawa, H., Takauchi, Y., Kawada, T., Sunagawa, K., 1997. A new, concise dialysis approach to assessment of cardiac sympathetic nerve terminal abnormalities. Am. J. Physiol. 272, H1182–H1187.

Yamazaki, T., Kawada, T., Akiyama, T., Kitagawa, H., Takauchi, Y., Yahagi, N., Sunagawa, K., 1997. ω-Conotoxin GVIA and desipramine insensitive norepinephrine efflux from cardiac sympathetic nerve terminal. Brain Res. 761, 329–332.

Yamazaki, T., Akiyama, T., Kawada, T., 1999. Effects of ouabain on in situ cardiac sympathetic nerve endings. Neurochem. Int. 35, 439–445.

Molecular Biology of the Cell
Vol. 14, 3553–3564, September 2003

Identification of Fer Tyrosine Kinase Localized on Microtubules as a Platelet Endothelial Cell Adhesion Molecule-1 Phosphorylating Kinase in Vascular Endothelial Cells[V]

Naoko Kogata,* Michitaka Masuda,* Yuji Kamioka,* Akiko Yamagishi,* Akira Endo,* Masato Okada,† and Naoki Mochizuki*‡

*Department of Structural Analysis, National Cardiovascular Center Research Institute, Suita, Osaka 565-8565, Japan; and †Department of Oncogene Research, Research Institute for Microbial Diseases, Osaka University, Osaka 565-0871, Japan

Submitted February 12, 2003; Revised May 10, 2003; Accepted May 22, 2003
Monitoring Editor: Richard Assoian

Platelet endothelial adhesion molecule-1 (PECAM-1) is a part of intercellular junctions and triggers intracellular signaling cascades upon homophilic binding. The intracellular domain of PECAM-1 is tyrosine phosphorylated upon homophilic engagement. However, it remains unclear which tyrosine kinase phosphorylates PECAM-1. We sought to isolate tyrosine kinases responsible for PECAM-1 phosphorylation and identified Fer as a candidate, based on expression cloning. Fer kinase specifically phosphorylated PECAM-1 at the immunoreceptor tyrosine-based inhibitory motif. Notably, Fer induced tyrosine phosphorylation of SHP-2, which is known to bind to the immunoreceptor tyrosine-based inhibitory motif of PECAM-1, and Fer also induced tyrosine phosphorylation of Gab1 (Grb2-associated binder-1). Engagement-dependent PECAM-1 phosphorylation was inhibited by the overexpression of a kinase-inactive mutant of Fer, suggesting that Fer is responsible for the tyrosine phosphorylation upon PECAM-1 engagement. Furthermore, by using green fluorescent protein-tagged Fer and a time-lapse fluorescent microscope, we found that Fer localized at microtubules in polarized and motile vascular endothelial cells. Fer was dynamically associated with growing microtubules in the direction of cell-cell contacts, where p120catenin, which is known to associate with Fer, colocalized with PECAM-1. These results suggest that Fer localized on microtubules may play an important role in phosphorylation of PECAM-1, possibly through its association with p120catenin at nascent cell-cell contacts.

INTRODUCTION

Platelet endothelial adhesion molecule-1 (PECAM-1) belongs to the immunoglobulin superfamily of cell adhesion molecules and is expressed on endothelial cells, platelets, leukocytes, and monocytes (Newman *et al.*, 1990). It consists of six extracellular immunoglobulin domains, a transmembrane domain, and an intracellular domain, which is tyrosine phosphorylated upon cellular activation (reviewed in Newman, 1999).

PECAM-1 functions not only as an intercellular adhesion-stabilizing molecule but also as an intracellular signal-triggering molecule by providing phosphotyrosines that bind to Src homology 2 (SH2)-containing molecules (Lu *et al.*, 1997; Masuda *et al.*, 1997; Jackson *et al.*, 1997b). Phosphorylation of PECAM-1 on Tyr663 and Tyr686 (the aa numbers in this study follow the number first reported in Newman *et al.*, 1990), each of which constitute an immunoreceptor tyrosine-based inhibitory motif (ITIM) (Newman, 1999), provides a docking site for the SH2-domain–containing protein phosphatase, SHP-2. PECAM-1 phosphorylation and subsequent association with SHP-2 have been demonstrated in many different cell types and in response to various activating

Article published online ahead of print. Mol. Biol. Cell 10.1091/mbc.E03–02–0080. Article and publication date are available at www.molbiolcell.org/cgi/doi/10.1091/mbc.E03–02–0080.

[V] Online version of this article contains video material for some figures. Online version is available at www.molbiolcell.org.

‡ Corresponding author. E-mail address: nmochizu@ri.ncvc.go.jp.

Abbreviations used: BAEC, bovine aortic endothelial cell; EGFP, enhanced green fluorescent protein; ERK, extracellular signal-regulated kinase; FBS, fetal bovine serum; FCH, Fps/Fes/Fer and CIP4 homology; Gab1, Grb2-associated binder-1; GFP, green fluorescent protein; HAEC, human aortic endothelial cell; IRES, internal ribosomal entry site; ITIM, immunoreceptor tyrosine-based inhibitory motif; KD, kinase defective; p120ctn, p120 catenin; PCR, polymerase chain reaction; PECAM-1, platelet endothelial cell adhesion molecule-1; SH, Src homology; WT, wild type.

stimuli (Sagawa *et al.*, 1997; Jackson *et al.*, 1997a,b; Cao *et al.*, 1998; Newton-Nash and Newman, 1999). We have demonstrated that PECAM-1 becomes tyrosine phosphorylated and binds SHP-2 in vascular endothelial cells exposed to fluid shear stress or osmotic shock (Harada *et al.*, 1995; Masuda *et al.*, 1997; Osawa *et al.*, 1997,2002).

The protein tyrosine phosphatase SHP-2 consists of amino-terminal tandem SH2 domains and a carboxy terminal phosphatase domain (Feng, 1999). It is involved in a variety of growth factor-mediated signaling events (Kazlauskas *et al.*, 1993; Deb *et al.*, 1998; Myers *et al.*, 1998; Maroun *et al.*, 2000). The two SH2 domains of SHP-2 bind to a bisphosphoryl tyrosine-based activation motif, found in Grb2-associated binder-1 (Gab1) and insulin receptor substrate-1, which fully potentiates the catalytic activity of SHP-2 (Cunnick *et al.*, 2001). In addition, an interaction between SHP-2 and Gab1 is required for epidermal growth factor receptor- or hepatocyte growth factor receptor-mediated activation of extracellular signal-regulated kinase (ERK) (Cunnick *et al.*, 2000; Schaeper *et al.*, 2000). We recently demonstrated that PECAM-1 is required for activation of ERK in vascular endothelial cells exposed to shear stress and osmotic shock and that both SHP-2 and Gab1 are recruited to the cell-cell border where PECAM-1 is phosphorylated in these cells (Osawa *et al.*, 2002).

A role for members of the Src family of protein tyrosine kinases in PECAM-1 tyrosine phosphorylation has been proposed on the basis of studies demonstrating that Src family tyrosine kinases could bind to and phosphorylate PECAM-1 in in vitro kinase assays (Lu *et al.*, 1997; Masuda *et al.*, 1997), that members of both Src and Csk families of protein tyrosine kinases could phosphorylate PECAM-1 upon overexpression in COS cells (Cao *et al.*, 1998), and that PECAM-1 tyrosine phosphorylation in stimulated platelets could be blocked by the selective Src family kinase inhibitor PP2 (Cicmil *et al.*, 2000; Ohmori *et al.*, 2001). In vascular endothelial cells exposed to hyperosmotic shock, however, inhibitors of Src family kinases failed to block PECAM-1 tyrosine phosphorylation (unpublished observation in Osawa *et al.*, 2002), suggesting that the kinase responsible for PECAM-1 tyrosine phosphorylation in mechanically stimulated endothelial cells may be different from those that phosphorylate PECAM-1 in other cells and under other conditions.

The nonreceptor protein-tyrosine-kinase Fer was originally isolated as an Fps (Fujinami poultry sarcoma)/*Fes* (feline sarcoma)-*r*elated protein, and it was thus named Fer (Letwin *et al.*, 1988). The Fps/Fes and Fer kinases share high structural homology: an amino-terminal Fps/Fes/Fer and CIP4 homology (FCH) domain followed by three tandem coiled-coil domains, an SH2 domain, and a carboxy-terminal tyrosine kinase domain (Greer, 2002). Fps/Fes is expressed mainly in hematopoietic cells, and to a lesser extent in vascular endothelial cells and neuronal cells, whereas Fer is ubiquitously expressed. The role of Fps/Fes has been extensively studied in cytokine-mediated signaling. In contrast, Fer is able to bind to and phosphorylate adherens junctional proteins, p120catenin (p120ctn) and β-catenin, and promote its dissociation from N-cadherin (Kim and Wong, 1995; Arregui *et al.*, 2000). Thus, Fer is thought to be involved principally in the regulation of cell-cell contacts, especially at the adherens junction (Rosato *et al.*, 1998).

In this study, we sought to identify the PECAM-1 phosphorylating kinase. We demonstrate that Fer is essential for engagement-dependent phosphorylation of PECAM-1 and show for the first time that Fer localizes at the peripheral microtubules in polarizing and migrating vascular endothelial cells. The association between Fer and microtubules seems to be critical to phosphorylation of PECAM-1 by recruiting Fer to p120ctn colocalized with PECAM-1 at nascent cell-cell contacts.

MATERIALS AND METHODS

Reagent and Antibodies

Protein A and G-Agarose were purchased from Calbiochem (La Jolla, CA). Type I collagen used for coating glass-base dishes was from Nitta Gelatin (Osaka, Japan). Anti-green fluorescent protein (GFP), anti-bovine-PECAM-1, and anti-phospho-bovine-PECAM-1 recognizing phospho-Tyr686 (hereafter, PY-PECAM-1) were developed in our laboratory as reported previously (Osawa *et al.*, 2002). Magnetic beads conjugated with anti-human PECAM-1 were obtained from Dynal ASA (Oslo, Norway). Anti-p120ctn, anti-human-PECAM-1, and anti-phosphotyrosine (PY100) were from Cell Signaling Technology (Beverly, MA). Anti-FLAG (M2) and anti-tubulin were from Sigma-Aldrich (St. Louis, MO), and anti-hemagglutinin (HA) was from Roche Diagnostics (Basel, Switzerland). Anti-SHP-2 was from Santa Cruz Biotechnology (Santa Cruz, CA). Anti-Gab1 was a generous gift from T. Hirano (Osaka University, Osaka, Japan).

Plasmids

Enhanced green fluorescent protein (EGFP)-PECAM-1 was constructed by inserting cDNA encoding bovine PECAM-1 without a stop codon in frame into EGFP-N1 (BD Biosciences Clontech, Palo Alto, CA). EGFP-Fer wild-type (WT) was an expression vector for amino-terminally EGFP-tagged WT Fer. pCXN2-FLAG-WT Fer or Fes was derived from pCAGGS eukaryotic expression vector and expressed FLAG-tagged Fer or Fes (Niwa *et al.*, 1991). A cDNA encoding a kinase-defective (KD) form of Fer containing an Asp to Arg substitution at position 743 (Craig *et al.*, 2001), or a cDNA encoding a form of Fer with a nonfunctional SH2 domain containing an Arg to Gln substitution at position 483 (R483Q) was amplified by polymerase chain reaction (PCR)-based mutagenesis and subcloned into pCXN2-FLAG (Nagashima *et al.*, 2002) and EGFP-C1 (BD Biosciences Clontech). HcRed-p120ctn was constructed by inserting p120ctn cDNA in frame into HcRed-C1 (BD Biosciences Clontech). cDNAs encoding truncated forms of Fer were amplified by PCR and ligated into EGFP-C1. pGEX-cytoplasmic-PECAM-1 was a bacterial expression vector and contained cDNA encoding glutathione *S*-transferase followed by cytoplasmic domain of PECAM-1 (aa 593–712) in frame. pcDNA-HA-SHP-2 was described previously (Osawa *et al.*, 2002). Either Tyr663 or Tyr686, and both of PECAM-1 were substituted for Phe by PCR-based mutagenesis (hereafter, Y663F, Y686F, and Y663/686F, respectively). Amplified PCR fragments were inserted into carboxy-terminally V5 epitope-tagging plasmids, pcDNA-DEST40, by using Gateway technology (Invitrogen, Carlsbad, CA). EGFP-Fes and its kinase-defective mutant were obtained from S. Yanagi (Kobe University, Kobe, Japan) (Mitsui *et al.*, 2002). All of the DNA fragments amplified by PCR were ligated into pCR-BluntII-TOPO vector or pENTR-D-TOPO vector (Invitrogen), and the sequence was confirmed with an ABI Prism 3700 (Applied Biosystems Japan, Tokyo, Japan).

Virus

pCXN2-FLAG-internal ribosomal entry site (IRES)-EGFP was constructed as reported previously (Nagashima *et al.*, 2002). PCR-am-

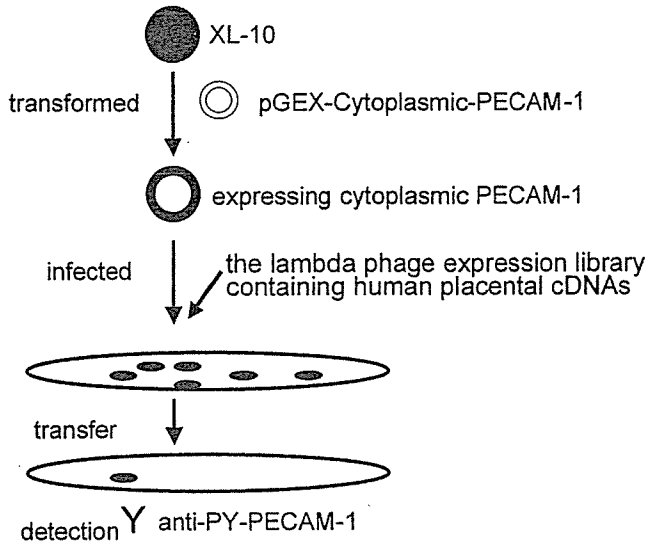

Figure 1. Schematic illustration of screening for PECAM-1–phosphorylating kinase. *E. coli*, XL-10 was first transformed by pGEX-cytoplasmic PECAM-1. The transformed bacteria were then infected with a lambda phage expression library containing human placental cDNAs. More than 5×10^5 plaques were transferred to the membrane and examined for the immunoreactivity with anti-PY-PECAM-1.

plified KD Fer cDNA was inserted into this vector, expressing both FLAG-tagged KD Fer and IRES-driven EGFP under bicistronic promoter. DNA encoding the promoter to EGFP was subcloned into pShuttle vector, and the expression cassette was transferred to pAdeno-X according to the manufacturer's protocol (BD Biosciences Clontech). We produced a recombinant adenovirus expressing both FLAG-tagged KD Fer and IRES-driven EGFP by transfecting human embryonic kidney (HEK)293 cells with pAdeno-X-KD Fer-IRES-EGFP. A recombinant adenovirus expressing GFP was obtained from H. Kurose (Kyushu University, Fukuoka, Japan).

Bacterial Expression Cloning

The protocol for expression cloning of PECAM-1 tyrosine phosphorylating kinase is illustrated in Figure 1. The *Escherichia coli* XL10-Gold was transformed with pGEX-cytoplasmic PECAM-1. Transformed bacteria were cultured overnight, collected by centrifugation at $3,500 \times g$ for 10 min, and resuspended in 10 mM $MgSO_4$. Then, resuspended bacteria were infected with the lambda phage library containing human placental cDNAs (TriplEx2; BD Biosciences Clontech). The protein expression was induced by 20 mM isopropyl β-D-thiogalactoside. The bacteria expressing both cytoplasmic PECAM-1 and library-promoted protein was lifted to the nitrocellulose membrane. The membranes were washed with Tris-buffered saline containing Tween 20 (25 mM Tris-hydrochloride pH 7.5, 150 mM NaCl, 2.5 mM KCl, and 0.05% Tween 20) and incubated with anti-PY-PECAM-1 at 4°C for 24 h. The immunoreaction was detected by peroxidase-conjugated anti-rabbit secondary antibody and visualized by an enhanced chemiluminescence method (Amersham Biosciences UK, Little Chalfont, Buckinghamshire, United Kingdom).

Cells, Transfection, and Infection

Human aortic endothelial cells (HAECs) were purchased from Cascade Biologics (Portland, OR) and maintained in HuMedia-EG2 (Kurabo, Kurashiki, Japan) supplemented with a growth additive set, as described previously (Nagashima *et al.*, 2002). Bovine aortic endothelial cells (BAECs) were cultured in DF1/2 as described previously (Osawa *et al.*, 1997). HEK293 cells were from the American Type Culture Collection (Manassas, VA) and cultured in DMEM (Invitrogen) supplemented with 10% fetal bovine serum (FBS), 2 mM L-glutamine. HEK293 cells were transfected with pAdeno-X-derived vectors to produce recombinant adenovirus using LipofectAMINE2000 (Invitrogen). HAECs cultured on a collagen-coated 35-mm-diameter glass-base dish (Asahi Techno Glass, Tokyo, Japan) were transfected with 3 μg of plasmid DNA by using LipofectAMINE PLUS reagent (Invitrogen) for 24 h or infected with adenovirus at the appropriate multiplicity of infection for >48 h before the stimulation.

Immunoprecipitation, Immunoblotting, and Cell Staining

Immunoprecipitation, immunoblotting, and immunocytochemistry were performed as reported previously (Nagashima *et al.*, 2002). Briefly, HAECs were washed with Tris-buffered saline containing 1 mM Na_3VO_4 and lysed in lysis buffer (150 mM NaCl, 20 mM Tris hydrochloride pH 7.5, 1.5 mM $MgCl_2$, 1 mM Na_3VO_4, 1% Triton X-100, 10 mM NaF, and protease inhibitor cocktail; Roche Diagnostics). Lysates were precleared by centrifugation at $15,000 \times g$ for 10 min, followed by immunoprecipitation by using antibodies indicated in the figures and protein A or G-Agarose (Calbiochem). Immunoprecipitates were subjected to SDS-PAGE and immunoblotting with antibodies as indicated in the figures. Proteins reacting with primary antibodies were visualized by an enhanced chemiluminescence system (Amersham Biosciences UK) for detecting peroxidase-conjugated species-matched secondary antibodies and quantitatively analyzed with an LAS-1000 system (Fuji Film, Tokyo, Japan). HAECs cultured on a collagen-coated glass-base dish and washed with phosphate-buffered saline were fixed by 4% paraformaldehyde at room temperature, followed by permeabilization with 0.1% Triton X-100. Permeabilized cells were incubated with anti-PECAM-1, anti-tubulin, or anti-p120ctn antibody. Proteins reacting with antibodies were detected with Alexa 546 goat anti-mouse IgG (Molecular Probes, Eugene, OR) for visualizing p120ctn and tubulin, and Alexa 488 goat anti-rabbit IgG for PECAM-1. Images for EGFP-tagged Fer and its mutants, PECAM-1, p120ctn, and tubulin were obtained by an Olympus IX71 fluorescent microscope (Olympus, Tokyo, Japan).

Engagement of PECAM-1

HAECs cultured on 60-mm collagen-coated dishes were uninfected or infected with either adenovirus expressing GFP or adenovirus expressing both KD Fer and IRES-driven EGFP for >48 h. HAECs on one dish were incubated with magnet beads conjugated with anti-PECAM-1 at 37°C for 30 min, lysed in lysis buffer, and collected on a magnet, whereas HAECs on another dish were lysed, incubated with beads conjugated with anti-PECAM-1 for 30 min at room temperature, and collected on a magnet. Collected proteins were subjected to SDS-PAGE and immunoblotted with PY100.

Time-Lapse Imaging

For time-lapse imaging, HAECs cultured on a collagen-coated glass-base dish were maintained in DMEM/F-12 (Invitrogen) supplemented with 10% FBS, 2 mM L-glutamine, 10 mM HEPES, and 1.2 g/l $NaHCO_3$ without phenol red. HAECs transfected with plasmids expressing fluorescence-tagged proteins were imaged on an Olympus IX71 inverted microscope with a 75-W Xenon arc lamp equipped with a cooled charge-coupled device camera, CoolSNAP-HQ (Roper Scientific, Trenton, NJ), and two filter changers, controlled by MetaMorph 4.6 software (Roper Scientific). Both the GFP image and the HcRed image were obtained through an XF2043

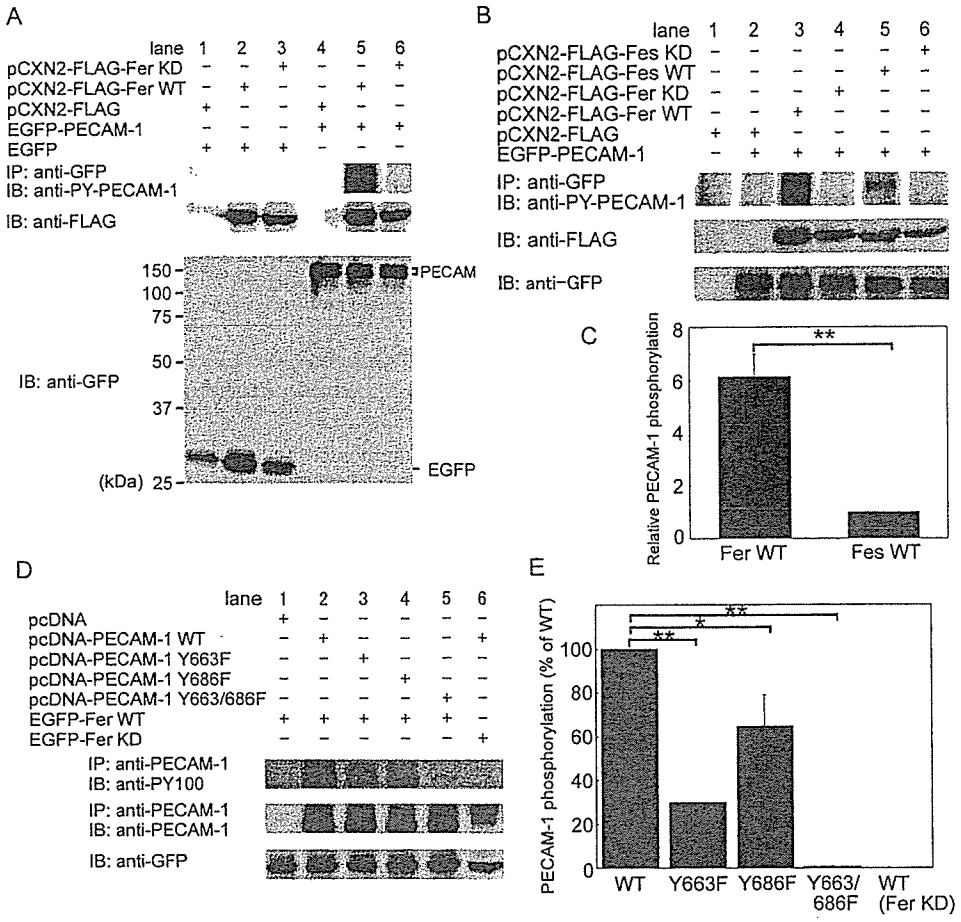

Figure 2. PECAM-1 is phosphorylated by Fer and, to a lesser extent, by Fes in vivo. (A) Lysate of 293T cells transfected with the plasmids indicated at the top were either immunoprecipitated (IP), followed by SDS-PAGE and immunoblotting (IB) with the antibodies as indicated, or directly subjected to SDS-PAGE and IB with the antibodies as indicated on the left. EGFP-N1 indicated as EGFP and pCXN2-FLAG were used as a negative control for EGFP-PECAM-1 and pCXN2-FLAG-Fer, respectively. The result is a representative of more than three independent experiments. Note that PECAM-1 is phosphorylated in 293T cells expressing WT Fer, as shown in lane 5. (B) Phosphorylation of PECAM-1 by Fer and Fes tyrosine kinases was analyzed as in A. Note that PECAM-1 is phosphorylated by Fer and, to a lesser extent, by Fes, as shown in lanes 3 and 5, respectively. (C) Quantitative analysis for PECAM-1 phosphorylation by Fer and Fes was performed. The relative intensity of phosphorylated PECAM-1 by Fer to that by Fes, as quantified by the use of LAS-1000 system (Fuji Film), is indicated as relative PECAM-1 phosphorylation. The data are expressed as averages with the SD. A significant difference between two groups determined by *t* test is indicated with a double asterisk ($p < 0.01$). (D) Cell lysate of 293T transfected with the plasmids as indicated at the top were used for examining the phosphorylation of Tyr663 and/or Tyr686 as analyzed in A. Note that Y663/686F was not phosphorylated by the overexpression of Fer as shown in lane 5. (E) Phosphorylation of Tyr663 and/or Tyr686 was quantitatively analyzed from the results obtained by the four independent experiments. The intensity of mutant PECAM-1 phosphorylated by Fer was compared with that of WT PECAM-1. The last column indicates that C-terminally V5 epitope-tagged PECAM-1 is not phosphorylated by KD Fer. Quantitative analysis was similarly performed as in C. A significant difference between two groups determined by *t* test is indicated with an asterisk ($p < 0.05$) and double asterisk ($p < 0.01$).

dichroic filter (Omega Optical, Brattleboro, VT) and a set of an S484/15 excitation filter and an S515/30 emission filter (Chroma Technology, Brattleboro, VT) for GFP, and a set of an S555/25 excitation filter and an S630/60 emission filter for HcRed. To monitor the localization of fluorescence-tagged proteins, we obtained a fluorescence image every 20 s. A series of time-lapse images were converted to video format by using MetaMorph 4.6 software.

RESULTS

Isolation and Identification of Fer as a PECAM-1 Phosphorylating Kinase

The cytoplasmic domain of PECAM-1 is phosphorylated upon PECAM-1 engagement and provides two SHP-2 binding sites at phosphorylated Tyr663 and Tyr686 (Osawa *et al.*, 2002). We aimed to identify the PECAM-1 phosphorylating kinase by using a bacterial expression cloning method and an antibody specific for a phosphotyrosine residue at position 686 of PECAM-1 (anti-PY-PECAM-1), as illustrated in Figure 1. *E. coli* expressing the cytoplasmic domain of PECAM-1 were infected with the lambda phage expression library containing human placental cDNAs, and at least 5×10^5 plaques were screened for immunoreactivity with anti-PY-PECAM-1. Six positive plaques were identified by immunoscreening. Five individual plaques contained the entire coding region of Fer. The other phage carried the cDNA of Src-family kinase, LynB. Src tyrosine kinase was not isolated by this screening, although previous studies have shown that Src phosphorylates PECAM-1 (Lu *et al.*, 1997).

PECAM-1 Is Phosphorylated by Fer and, To a Lesser Extent, by Fes

To test whether Fer can phosphorylate PECAM-1 in vivo, we examined whether cotransfection of PECAM-1 with WT or KD Fer results in PECAM-1 tyrosine phosphorylation as detected with anti-PY-PECAM-1 in 293T cells. Carboxy-terminally EGFP-tagged PECAM-1 was phosphorylated by WT Fer (Figure 2A, lane 5) but not KD Fer (Figure 2A, lane 6), whereas EGFP alone used as a negative control was not

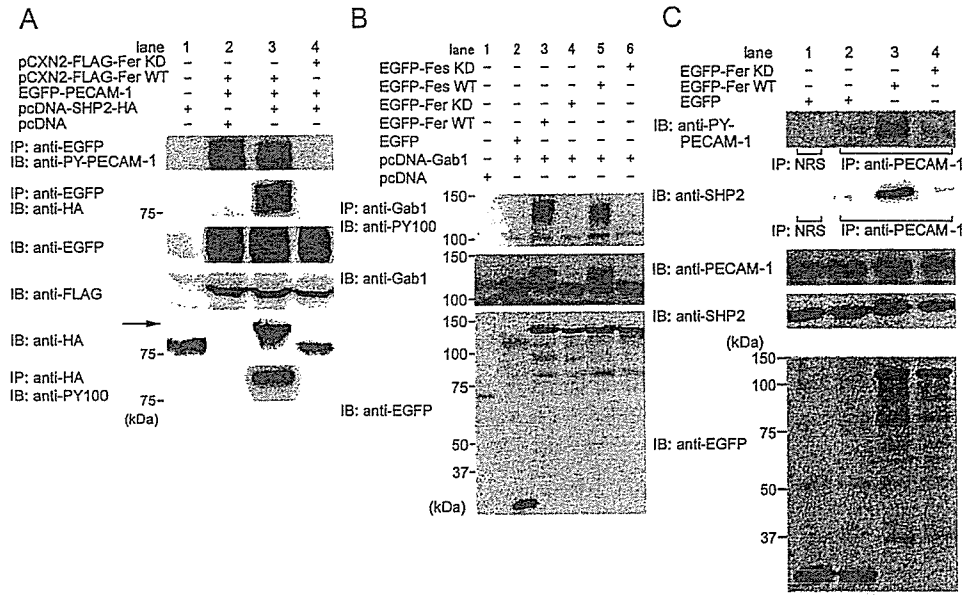

Figure 3. Fer not only phosphorylates PECAM-1, resulting in an increased association of SHP-2 and PECAM-1, but also induces the phosphorylation of SHP-2 and Gab1. (A) 293T cells were transfected with the plasmids, as indicated at the top. Cell lysates were subjected to immunoprecipitation (IP) followed by SDS-PAGE and immunoblotting (IB) or IB, as indicated on the left. Note that HA-tagged SHP-2 is detected in the immunoprecipitates with PECAM-1 precipitated by anti-GFP, as shown in lane 3. Furthermore, SHP-2 is detected as an upper-shifted band on an immunoblot with anti-HA, and immunoprecipitates by anti-HA antibody were detected by anti-phosphotyrosine antibody (PY100), indicating that SHP-2 is phosphorylated by Fer. (B) 293T cells were transfected with the plasmids, as indicated at the top. Cell lysates were analyzed by IB with antibodies indicated on the left. Note that Gab1 on the immunoblot with anti-Gab1 was detected as an upper-shifted band and the immunoprecipitates by anti-Gab1 antibody was detected by PY100, indicating that Fer induces the phosphorylation of Gab1. (C) BAECs cultured at 90% confluence were transfected with the plasmids, as indicated at the top. Cell lysates were immunoprecipitated (IP) with either normal rabbit serum (NRS) used as a negative control or anti-PECAM-1, as indicated beneath the panels, followed by SDS-PAGE and immunoblotting with the antibodies, as indicated on the left. Remaining lysates were subjected to SDS-PAGE and immunoblot probed with the antibodies indicated on the left. Note that more PECAM-1 is phosphorylated, that the amount of SHP-2 associating with PECAM-1 is increased, and that PECAM-1 is phosphorylated even without overexpression of Fer (lane 2), presumably depending on the cell-cell contact because of the confluence.

phosphorylated by either WT Fer or KD Fer, as determined by immunoprecipitation with anti-GFP followed by immunoblotting with anti-phosphotyrosine antibody (our unpublished data).

We performed a similar experiment by using Fes, a tyrosine kinase closely related to Fer. WT Fes phosphorylated PECAM-1 in 293T cells, albeit to a lesser extent than WT Fer (Figure 2B, lanes 3 and 5). The phosphorylation of PECAM-1 by either Fer or Fes was quantified as in Figure 2C. The difference in phosphorylation could be explained by the difference in the substrate specificity or localization between Fer and Fes.

Bovine PECAM-1 contains six tyrosine residues in its cytoplasmic domain of which only the two ITIM tyrosine residues, Tyr663 and Tyr686, have been reported to be phosphorylated (Jackson *et al.*, 1997a; Cao *et al.*, 1998). To examine which tyrosine residues are phosphorylated by Fer, we used the carboxy-terminally V5 epitope-tagged PECAM-1 mutants Y663F, Y686F, and Y663/686F as a substrate, and we used anti-phosphotyrosine antibody (PY100) instead of anti-PY-PECAM-1 (Figure 2D). 293T cells were transfected with each of these mutant-expressing vectors and a Fer-expression vector. Y663/686F was not phosphorylated (Figure 2D, lane 5), whereas WT (Figure 2D, lane 2), Y663F (Figure 2D, lane 3), and Y686F (Figure 2D, lane 4) forms of PECAM-1 were all tyrosine phosphorylated by WT Fer. Quantification of phosphorylation of both WT and mutant forms of PECAM-1 by Fer revealed that the levels of phosphorylation of Y663F and Y686F mutant forms of PECAM-1 were decreased by 70 and 30%, respectively. These results indicate that Fer phosphorylates both Tyr663 and Tyr686 but that the former is the preferred site.

Fer not Only Phosphorylates PECAM-1 to Induce the Association of SHP-2 with PECAM-1 but also Induces the Phosphorylation of SHP-2 and Gab1

The ITIM motif of PECAM-1 is known to be a docking site for SHP-2. We have previously shown that phosphorylated PECAM-1 associates with SHP-2 in BAECs upon PECAM-1 engagement (Osawa *et al.*, 2002). Thus, we tested whether the PECAM-1 phosphorylation mediated by Fer determines the association between PECAM-1 and SHP-2. HA-tagged SHP-2 was coimmunoprecipitated with EGFP-tagged PECAM-1 phosphorylated by Fer (Figure 3A, lane 3), whereas it was not in KD-Fer transfected 293T cells (Figure 3A, lane 4). In addition, we noticed that HA-tagged SHP-2 was detected as an upward-shifted band on an immunoblot, as indicated by the arrow in Figure 3A, which suggested that phosphorylation of SHP-2 might be induced by Fer. We proceeded to examine whether the upward-shifted band

was tyrosine phosphorylated SHP-2. Immunoprecipitates by anti-HA antibody were detected by anti-phosphotyrosine antibody (PY100), indicating that SHP-2 was tyrosine phosphorylated by WT Fer (Figure 3A, bottom, lane 3). We also observed that SHP-2 coimmunoprecipitated with EGFP-PECAM-1 was tyrosine phosphorylated (our unpublished data). We have demonstrated that mechanical stress-promoting PECAM-1 phosphorylation induces the translocation of Gab1 to cell-cell contacts with SHP-2 (Osawa *et al.*, 1997). Gab1 contains the bisphosphoryl tyrosine-based activation motif as a binding site for SHP-2. We examined whether the phosphorylation of Gab1 was induced by Fer (Figure 3B). Gab1 in lysates from cells transfected with WT Fer and WT Fes was detected as upward-shifted bands on an immunoblot similar to SHP-2 (Figure 3B, middle, lanes 3 and 5). These upward-shifted bands represented tyrosine phosphorylated Gab1, as demonstrated by immunoprecipitation by anti-Gab1 followed by anti-phosphotyrosine immunoblotting (Figure 3B, top, lanes 3 and 5). WT Fes, to a lesser extent than WT Fer, induced tyrosine phosphorylation of Gab1 (Figure 3B, lane 5). These results suggest that Fer not only functions as a tyrosine kinase for PECAM-1 but also that Fer modulates the downstream signaling of PECAM-1 by inducing phosphorylation of SHP-2 and Gab1.

SHP-2 Binds PECAM-1 Phosphorylated by Fer in BAECs

PECAM-1 phosphorylated upon mechanical stress recruits SHP-2 in BAECs (Osawa *et al.*, 2002). To test whether endogenous SHP-2 binds to PECAM-1 phosphorylated by Fer, we examined the association in BAECs. BAECs cultured at subconfluence were transfected with plasmids expressing Fer. PECAM-1 was phosphorylated and associated with SHP-2 in mock-transfected cells (Figure 3C, lane 2), likely as a result of cell contact-induced homophilic binding of PECAM-1. Notably, the more PECAM-1 was phosphorylated by Fer, the more SHP-2 was associated with PECAM-1 in Fer-transfected cells (Figure 3C, lane 3). We could not detect an upward-shifted band of endogenous SHP-2 due to the low transfection efficiency in BAECs.

Fer Is Indispensable for Phosphorylation of PECAM-1 upon Engagement

To confirm the requirement of Fer for PECAM-1 engagement-dependent phosphorylation, we used the application of anti-PECAM-1–coated beads to HAECs to mimic homophilic PECAM-1 binding. To determine whether Fer is required for anti-PECAM-1 antibody-induced PECAM-1 phosphorylation, we evaluated the effect of expressing KD Fer, which presumably functions as a dominant negative inhibitor of endogenous Fer activity, on PECAM-1 phosphorylation. HAECs were infected with either adenovirus expressing GFP or adenovirus expressing FLAG-tagged KD Fer and IRES-driven EGFP for >48 h, when >90% of the cells were infected, as determined by the expression of GFP (Figure 4, bottom). PECAM-1 became phosphorylated in cells uninfected and in cells infected with GFP-expressing adenovirus upon incubation with anti-PECAM-1 beads (Figure 4, lanes 2 and 4), whereas PECAM-1 was not phosphorylated in cells infected with adenovirus expressing both KD-Fer and IRES-driven EGFP (Figure 4, lane 6). These results indicate that Fer is required for anti-PECAM-1 antibody-induced phosphorylation of PECAM-1.

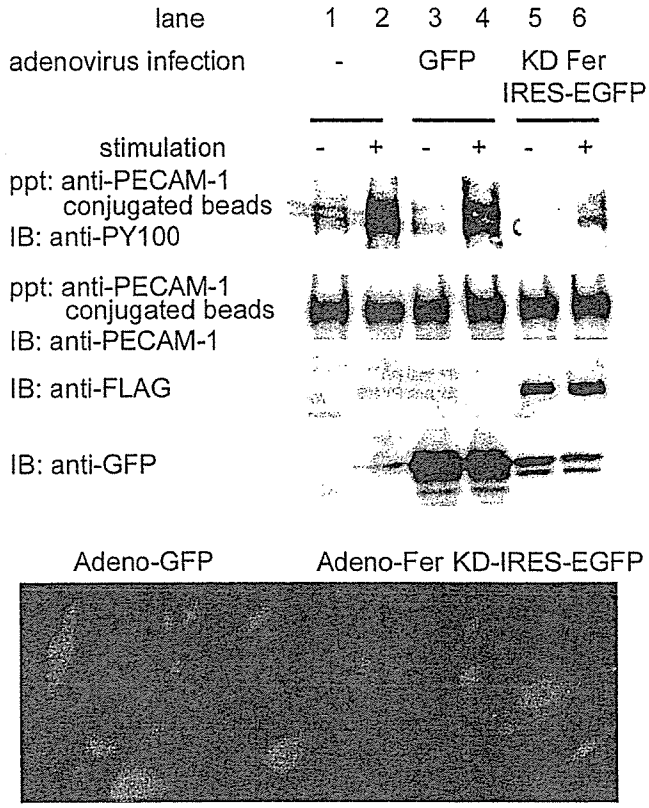

Figure 4. Engagement-dependent phosphorylation of PECAM-1 mimicked by applying PECAM-1 activating antibody. HAECs were uninfected (lanes 1 and 2) or infected with either adenovirus expressing GFP (lanes 3 and 4) or adenovirus expressing both KD Fer and IRES-driven EGFP (lanes 5 and 6). Cell lysates were collected on anti-human-PECAM-1 antibody-conjugated beads without stimulation (−) or after stimulation (+), as described in MATERIALS and METHODS. Proteins bound to the beads were eluted with SDS-sample buffer, subjected to SDS-PAGE, and immunoblot probed with antibodies, as indicated on the left. Cell lysates were analyzed for expression of FLAG-tagged KD Fer or GFP as indicated at the left. Bottom, infection efficiency of adenovirus, as shown by GFP-positive cells. The result is a representative of more than three independent experiments.

Fer Localizes to Microtubules in Vascular Endothelial Cells

Fer contains an FCH domain, which is thought to be a microtubule-targeting motif (Aspenstrom, 1997; Tian *et al.*, 2000). Previously, Fer and Fes were reported to be localized in the nucleus (Hao *et al.*, 1991; Yates *et al.*, 1995). Another report showed Fes in the *trans*-Golgi network and Fer in the cytoplasm (Zirngibl *et al.*, 2001). Hence, we examined the localization of Fer and Fes by using EGFP-tagged Fer and Fes in HAECs. EGFP-tagged WT Fer partially localized with tubular structures in the protruded zone of the cell. We tested the colocalization of Fer with microtubules by using an anti-tubulin antibody. Indeed, Fer was colocalized with

microtubules in protrusions of polarized cells (Figure 5A, top). In sharp contrast, EGFP-tagged WT Fes was partially localized with microtubules, particularly in the central region of microtubules but not on peripheral microtubules (Figure 5A, bottom). This distinct localization of Fer and Fes may affect the phosphorylation efficiency of PECAM-1 at cell-cell contacts in the endothelial cells.

Vascular endothelial cells are motile on the collagen-coated dishes and polarize when they migrate. We monitored EGFP-tagged WT Fer in living cells by using a time-lapse microscope. HAECs were transfected with EGFP-tagged WT Fer and cultured on collagen-coated glass-bottom dishes in DMEM with 10% FBS. Under these conditions, HAECs were motile and in perpetual motion until cells reached confluence. At the point when we started monitoring, Fer was localized with microtubules in the polarizing cell in contact with an adjacent cell indicated by the circle in Figure 5B (time 0 min). As the cell began to move toward the cell indicated by the triangle, EGFP-tagged Fer was relocated at newly assembling microtubules, as indicated by the arrow in Figure 5B (time 20 min). EGFP-tagged Fer disappeared from the retracting tail, which lost cell-cell contact with the cell indicated by the circle in Figure 5B and localized at the newly assembling microtubules in the protrusion that contacts another cell as indicated by the triangle in the figure (time 60 and 120 min, respectively). Notably, newly assembled microtubules indicated by EGFP-tagged Fer reached the cell-cell contact points (Figure 5B, and Video 1). These data indicate that the localization of Fer depends on the assembly and disassembly of microtubules and that Fer is dynamically recruited to nascent microtubules in the protruding side from the retracting tail and may function at the leading edge of the cell.

FCH Domain Is Dispensable for Fer Localization on the Microtubules

To determine the microtubule-targeting domain of Fer, we constructed a panel of EGFP-tagged truncated and mutated Fer clones (Figure 6A). Recently, a domain conserved among *B*in1, *A*mphiphysin, and a yeast protein, *R*SV, has been reported and designated as a BAR domain named after these molecules (Ge and Prendergast, 2000); however, its function has not yet been elucidated. Fer contains this domain between the first and the third coiled-coil domain.

To examine whether EGFP-tagged mutants of Fer were correctly constructed, we transfected 293T cells with a panel of plasmids encoding EGFP-tagged mutants. EGFP-tagged molecules were detected at the expected molecular weight, as demonstrated by an immunoblot probed with anti-GFP antibody (Figure 6B).

The FCH domain has been thought to be a microtubule-targeting domain because CIP4 localizes on the microtubules (Tian *et al.*, 2000). Neither EGFP-tagged KD Fer, nonfunctional SH2-mutant (R483Q) of Fer, nor EGFP-tagged FCH of Fer localized on microtubules. Unexpectedly, dFCH did localize on microtubules in polarized cells as did WT Fer. Apparently, deletion mutants lacking the first (dCC1) or all (dCC2) of the coiled-coil domains, or those containing only the SH2 and kinase domain (SH2-K), were not capable of targeting Fer to microtubules (Figure 6). dCC2 and SH2-K localized in the nucleus, probably as a result of a bipartite nuclear localization signal between aa 540 and aa 557 (Ben

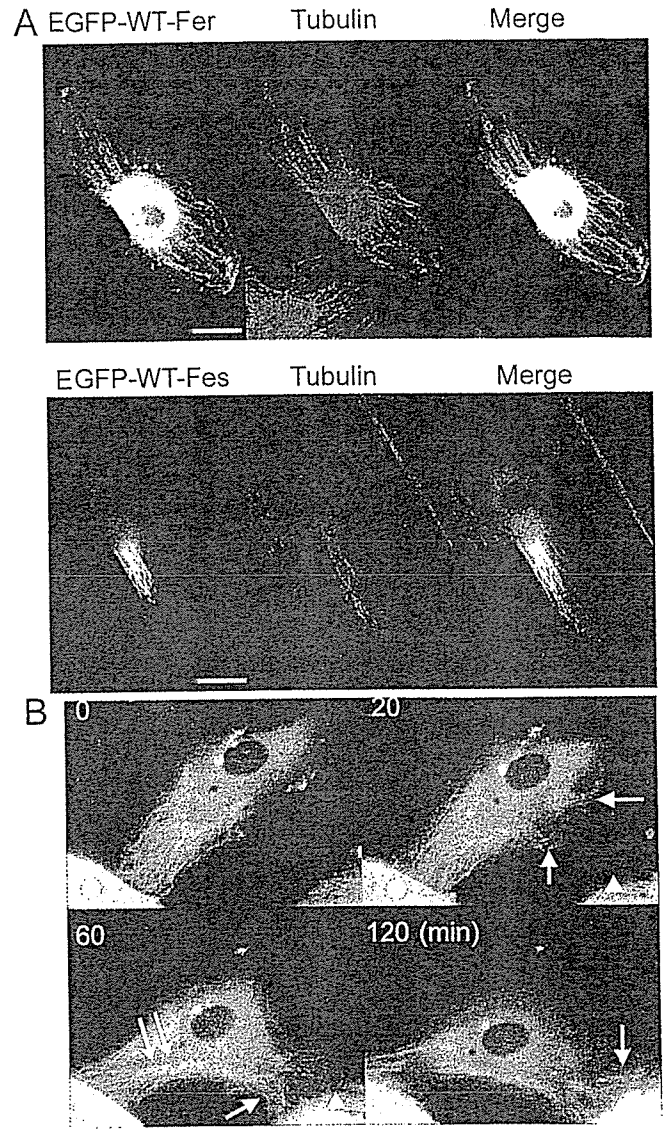

Figure 5. Fer localizes to the microtubules in the polarizing area of HAECs. (A) HAECs expressing EGFP-tagged Fer (top) or EGFP-tagged Fes (bottom) plated on the collagen-coated glass-base dish were fixed with 4% paraformaldehyde, permeabilized with 0.1% Triton X-100, and incubated with anti-tubulin antibody. Immunoreactive protein was visualized by Alexa546 goat anti-mouse IgG. Images for GFP and Alexa546 were obtained using an Olympus IX71 microscope. An image for EGFP-tagged Fer or Fes (green) and an image for tubulin (red) were superimposed (merge). Bar, 20 μm. (B) A series of time-lapse images for EGFP-tagged Fer are shown. Images were obtained at the indicated time after the beginning of the observation. Arrows indicate EGFP-Fer localized at the microtubules in the polarizing area of HAECs. Double arrows indicate the dispersion of EGFP-tagged Fer from the microtubules in the retracting area (also see Video 1). Neighboring cells are marked by either a circle or a triangle. Time-lapse images were obtained using an Olympus IX71 equipped with a cooled charge-coupled device camera and two filter changers controlled by MetaMorph 4.6. A series of images were converted to a video (Video 1).

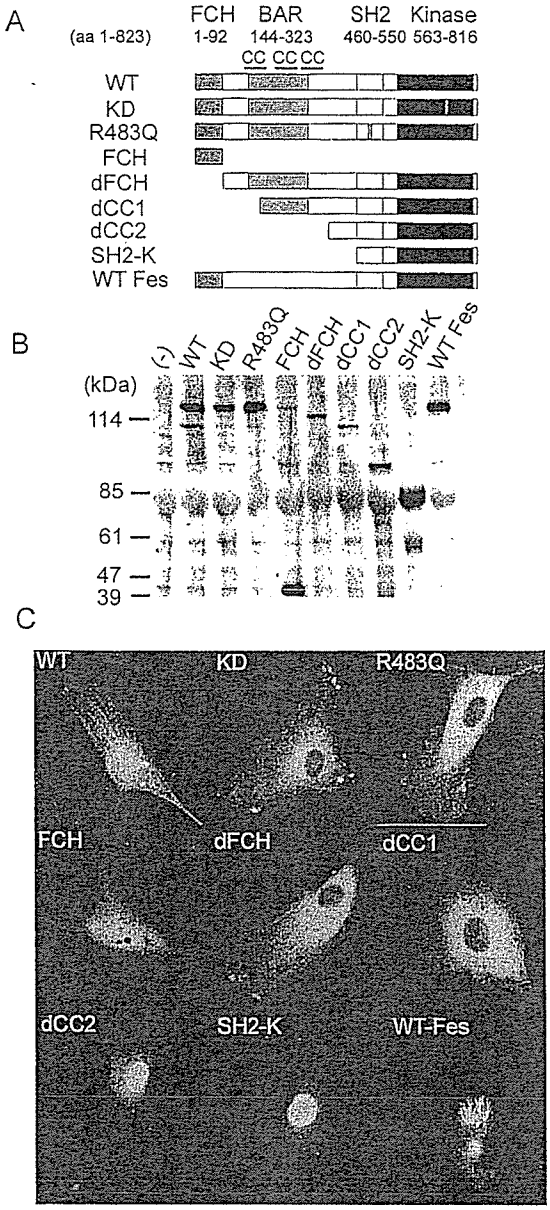

Figure 6. Fer requires coiled-coil, SH2, and kinase domains for localizing to the microtubules in vascular endothelial cells. (A) Fer consists of FCH, BAR flanked by the first and the third coiled-coil domain, SH2, and tyrosine kinase domain, as schematically illustrated. The amino acid number encoding each domain is indicated at the top. The kinase defective mutation (KD) and SH2 mutation (R483Q) of Fer are shown as small dark boxes. dFCH, dCC1, and dCC2 denote deletion of the FCH domain, that of the FCH and the first coiled-coil domain, and that of the FCH and all coiled-coil domain, respectively. SH2-K denotes the deletion mutant of Fer consisting of the SH2 and tyrosine kinase domains. (B) 293T cells were transfected with the plasmids encoding amino-terminally EGFP-tagged DNA, as indicated at the top. Cell lysates were subjected to SDS-PAGE, followed by immunoblot probed with anti-GFP antibody. (C) HAECs were transfected with the plasmids used in B and imaged through an Olympus IX71 fluorescent microscope. Note that WT Fer and dFCH localize on the polarized microtubules, whereas mutants lacking the first coiled-coil domain, KD, or R483Q, do not localize on the microtubules.

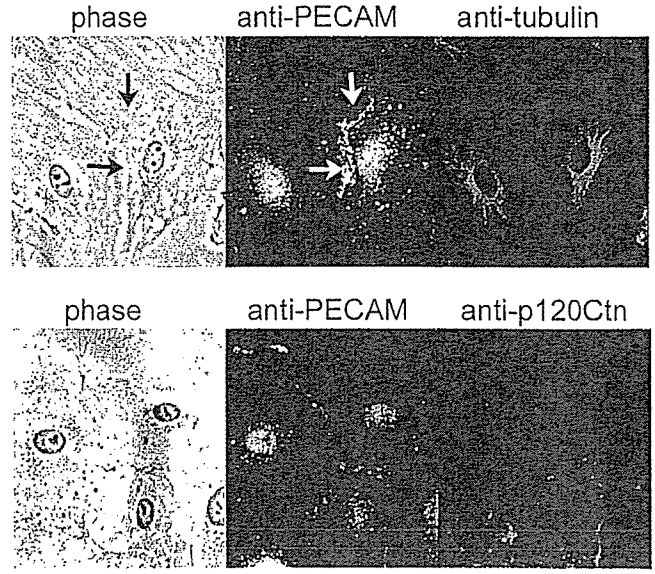

Figure 7. Microtubules are organized toward the cell-cell contact, where PECAM-1 colocalizes with p120ctn in HAECs. HAECs cultured on a glass-base dish were permeabilized with 0.1% Triton X-100 and immunostained with both rabbit anti-PECAM-1 antibody and mouse anti-tubulin antibody (top) or mouse anti-p120ctn antibody (bottom). PECAM-1 (green) and tubulin (top, red)/p120ctn (bottom, red) were visualized by fluorophore-labeled species-matched Alexa secondary antibody. PECAM-1 at cell-cell contact is indicated by the arrows (top). Note that the microtubules are organized toward the cell-cell contact, which is revealed by the immunostaining with PECAM-1 (top) and that PECAM-1 colocalizes with p120ctn (bottom). Phase, phase contrast view.

Dor *et al.*, 1999). These results suggest that the coiled-coil in the BAR domain, the SH2 domain, and the kinase domain, but not FCH domains are required for localization of Fer to microtubules.

PECAM-1 Colocalized at Nascent Cell-Cell Contact with p120ctn

To understand the cellular mechanism by which Fer colocalized with microtubules can phosphorylate PECAM-1, we examined the localization of PECAM-1, microtubules, and p120ctn, because a previous study has demonstrated that Fer binds to p120ctn via the coiled-coil domain and phosphorylates it (Kim and Wong, 1995). PECAM-1 localized at nascent cell-cell contacts, as indicated by the arrows in Figure 7 (top). Notably, microtubules were organized toward cell-cell contacts, as demonstrated by the immunostaining by using an anti-tubulin antibody (Figure 7). p120ctn binds to the conserved cadherin juxtamembrane domain, resulting in localization at cell-cell contacts, in particular at adherens junctions (Anastasiadis and Reynolds, 2000). We further examined the localization of PECAM-1 together with p120ctn and found that p120ctn colocalized with PECAM-1 at cell-cell contacts (Figure 7, bottom).

To decipher the localization of Fer to microtubules in living cells, we monitored the accumulation of p120ctn at the cell-cell contact and Fer on the microtubules by EGFP-tagged Fer and

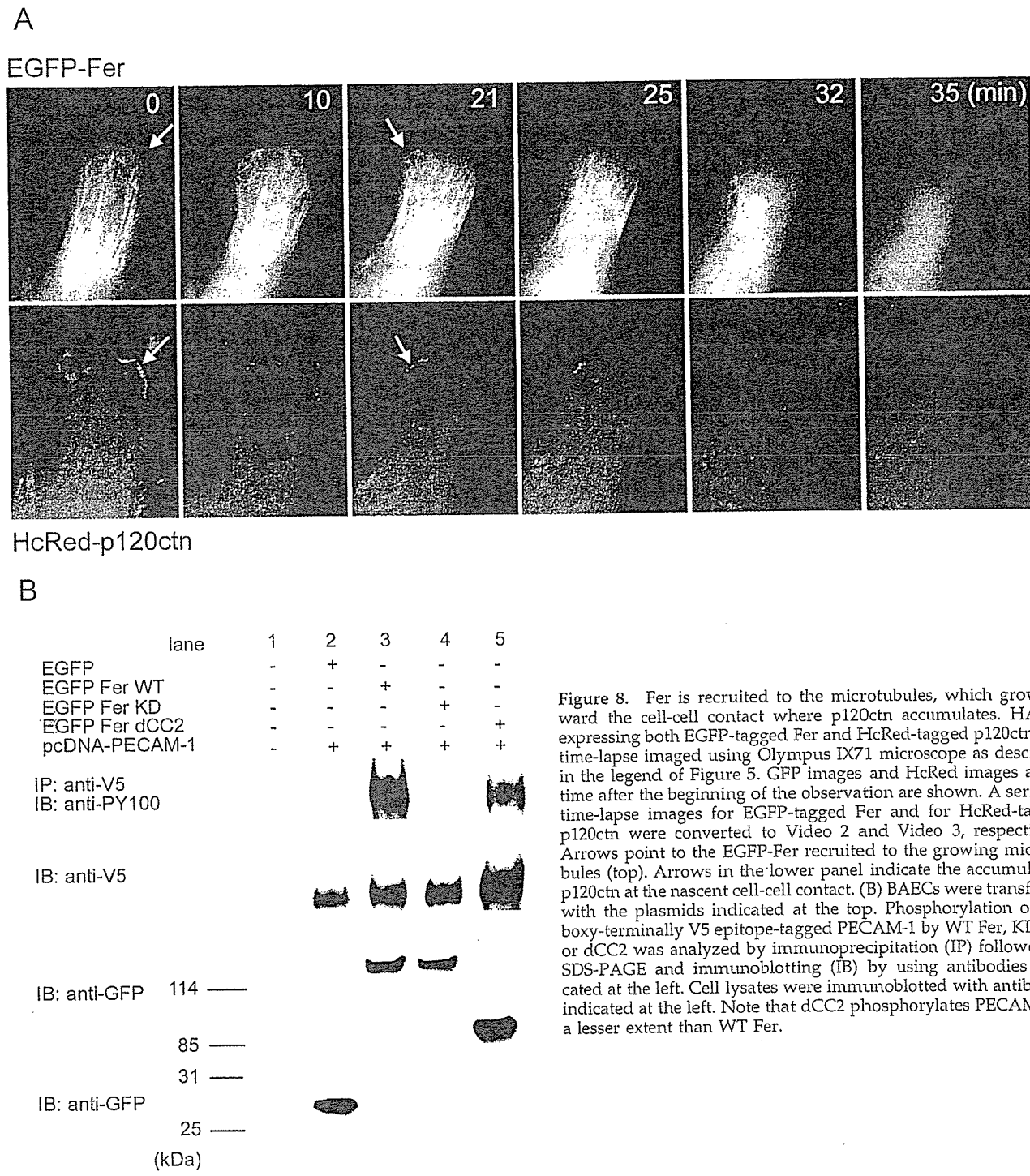

Figure 8. Fer is recruited to the microtubules, which grow toward the cell-cell contact where p120ctn accumulates. HAECs expressing both EGFP-tagged Fer and HcRed-tagged p120ctn was time-lapse imaged using Olympus IX71 microscope as described in the legend of Figure 5. GFP images and HcRed images at the time after the beginning of the observation are shown. A series of time-lapse images for EGFP-tagged Fer and for HcRed-tagged p120ctn were converted to Video 2 and Video 3, respectively. Arrows point to the EGFP-Fer recruited to the growing microtubules (top). Arrows in the lower panel indicate the accumulating p120ctn at the nascent cell-cell contact. (B) BAECs were transfected with the plasmids indicated at the top. Phosphorylation of carboxy-terminally V5 epitope-tagged PECAM-1 by WT Fer, KD Fer, or dCC2 was analyzed by immunoprecipitation (IP) followed by SDS-PAGE and immunoblotting (IB) by using antibodies indicated at the left. Cell lysates were immunoblotted with antibodies indicated at the left. Note that dCC2 phosphorylates PECAM-1 to a lesser extent than WT Fer.

HcRed-tagged p120ctn in motile HAECs by using a time-lapse microscope. EGFP-tagged Fer localized to assembling microtubules at the lamellipodia in the protruding zone of the HAEC, as indicated by the arrows in Figure 8. In addition, during the shift from the protruding zone to the retracting zone of HAECs, EGFP-tagged Fer disappeared in the retracting zone (Figure 8, top, and Video 2). In the same cell, HcRed-tagged p120ctn began to accumulate at the cell-cell contacts with adjacent cells (Figure 8, bottom, and Video 3). On the disruption of cell-cell contact, DsRed-tagged 120ctn dispersed from the cell-cell contact. These findings suggest that upon cell-cell contact, p120ctn accumulates at the adherens junction and recruits

Fer on the microtubules to adherens junctions. To examine whether p120ctn is involved in phosphorylation of PECAM-1 by Fer, we compared the phosphorylation of PECAM-1 by WT Fer and that by dCC2 lacking coiled-coil domains required for the association with p120ctn. Notably, the efficiency of PECAM-1 phosphorylation was less in cells transfected with dCC2 than in those transfected with WT Fer (Figure 8B, lanes 3 and 5). We observed that autophosphorylation of dCC2 was not perturbed by the removal of coiled-coil domains (our unpublished data). These results suggest that the coiled-coil domain-mediated interaction between Fer and p120ctn may contribute to phosphorylation of PECAM-1 by Fer at cell-cell contacts.

DISCUSSION

PECAM-1 functions as an adhesive molecule and as a signaling mediator during cell-cell contact (Newman, 1997). Phosphorylation of PECAM-1 is required for triggering intracellular signaling (Newman, 1999). Herein, we have identified Fer tyrosine kinase as a PECAM-1 phosphorylating kinase and as an inducer for SHP-2 and Gab1 phosphorylation. In addition, we have suggested an important role in localization of Fer to microtubules for phosphorylation of PECAM-1.

Bacterial expression cloning enabled us to isolate Fer kinase as a PECAM-1 phosphorylating kinase. This method is advantageous in screening kinases that directly phosphorylate the cytoplasmic domain of PECAM-1. Previous data have shown that Src is capable of phosphorylating and binding to PECAM-1 by in vitro kinase assays and in an overexpression study (Lu *et al.*, 1997; Cao *et al.*, 1998). In our laboratory, phosphorylation of PECAM-1 induced by mechanical stretch was not perturbed in the presence of the Src family kinase inhibitor PP2 (unpublished observation in Osawa *et al.*, 2002). Thus, Fer seems to be the best candidate for a PECAM-1–phosphorylating kinase. This notion is supported by the evidence that Tyr663 of PECAM-1 is a preferred site for Fer (Figure 2E), whereas Tyr686 is a preferred site for Src and Csk families of protein tyrosine kinase (Cao *et al.*, 1998). Because mice harboring inactivating mutation of Fer are viable (Craig *et al.*, 2001), Fes and/or LynB, both of which have been shown to phosphorylate PECAM-1, may compensate for the defects in these mice.

The physiological consequence of PECAM-1 phosphorylation remains unknown. We previously demonstrated that phosphorylated PECAM-1 triggered SHP-2-mediated intracellular signaling, including recruitment of Gab1 and ERK activation in vascular endothelial cells (Masuda *et al.*, 1997; Osawa *et al.*, 2002). In the present study, we have shown that Fer can induce phosphorylation of both SHP-2 and Gab1 (Figure 3). Moreover, Gab1 and SHP-2 cooperatively function to activate ERK and to induce branching morphogenesis, thereby triggering active cell motility in Madin-Darby canine kidney cells (Schaeper *et al.*, 2000). ERK is involved in actomyosin contractility, which is essential for cell migration, by phosphorylating myosin light chains (Cheresh *et al.*, 1999). In addition, cortactin, a substrate of Fer kinase, participates in membrane ruffling by binding to F-actin (Kim and Wong, 1998). A deficiency of cortactin phosphorylation and a migration defect were found in Fer-deficient fibroblasts and in Fer-deficient mast cells, respectively (Craig *et al.*, 2001; Craig and Greer, 2002). Collectively, Fer seems to orchestrate the downstream signaling of PECAM-1, leading to cell migration by phosphorylating signaling molecules regulating cell motility.

Most cytoplasmic protein tyrosine kinases contain conserved domains such as SH2, SH3, and pleckstrin homology besides tyrosine kinase domain (Blume-Jensen and Hunter, 2001). Among protein tyrosine kinases, Fer and Fes are the only family members that contain an FCH domain, the function of which has not yet been defined. Because the FCH domain of CIP4 binds to microtubules (Tian *et al.*, 2000), the amino-terminal FCH of Fer and Fes has been expected to function as a microtubule-targeting domain (Greer, 2002). We found that GFP-tagged Fer and Fes partially colocalized with microtubules and demonstrated that microtubule targeting of Fer was perturbed by deletion of the coiled-coil domain. Intriguingly, the removal of the FCH domain from Fer did not perturb the localization of Fer to microtubules, as shown in Figure 6. These data indicate that the FCH domain is not the sole microtubule-targeting domain. EGFP-tagged Fer localized at both proximal and peripheral microtubules in the polarizing zone toward the leading edge. In contrast, Fes localized at proximal microtubules. The distinct localization of Fer and Fes may account for efficiency of the PECAM-1 phosphorylation. Moreover, the evidence that Fer localized on vesicular structures near proximal microtubules such as GFP-tagged Fes (Figure 5B) coincides with the previous report demonstrating the localization of Fes/Fps to vesicular structures and partial colocalization with several Rab proteins (Zirngibl *et al.*, 2001).

We have demonstrated for the first time that Fer localizes to microtubules, as shown in Figure 5. We developed an antibody against Fer to examine the localization of endogenous Fer in endothelial cells. Endogenous Fer could not be detected on microtubules by using the antibody we developed, raising two possibilities; one is that endogenous Fer that is inactive without any stimulation may not localize to microtubules, and the other is simply that the antibody is not sensitive enough to detect the endogenous Fer. The former possibility is supported by the evidence that overexpressed Fer is autophosphorylated in fibroblasts (Rosato *et al.*, 1998) and our data that EGFP-tagged WT Fer but not KD Fer localized to microtubules. In contrast, Hao *et al.*, 1991 and Yates *et al.*, 1995 reported that Fer and Fes localize in the nucleus. Although our results did not coincide with these previous reports, the localization of Fer may depend on whether PECAM-1 is activated.

Microtubules are polarized in the migrating cells and grow forward to the leading edge (Wittmann and Waterman-Storer, 2001). In vascular endothelial cells, microtubules detected by EGFP-tagged Fer grew toward neighboring cells and reached cell-cell contacts, where PECAM-1 accumulated (Figures 5B and 7). As shown in Figure 8, p120ctn also accumulated at nascent cell-cell contacts toward which microtubules were growing. p120ctn can associate with Fer via its coiled-coil domain (Kim and Wong, 1995). In addition, we found that dCC2 lacking p120ctn association-domain phosphorylated PECAM-1 to a lesser extent than WT (Figure 8B). Thus, an association between Fer and p120ctn at nascent cell-cell contacts seems to contribute to phosphorylation of PECAM-1.